Supplementary Information

Self-Assembly of Macromolecules within Single Topological Defects of Nematic Solvents

JungHyun Noh[a,‡], Wei Cao[b,‡], Hao Sun[b], Yu Yang[a,c], Nathan C. Gianneschi[b,*], and Nicholas L. Abbott[a,*]

[a]School of Chemical and Biomolecular Engineering, Cornell University, Ithaca, New York 14853, United States

[b]Department of Chemistry, Materials Science & Engineering, Biomedical Engineering, Pharmacology, International Institute for Nanotechnology, Simpson Querrey Institute, Chemistry of Life Processes Institute and the Lurie Cancer Center, Northwestern University, Illinois 60208, United States

[c]Department of Chemical and Biological Engineering, University of Wisconsin-Madison, Madison, Wisconsin 53706, United States

‡These authors contributed equally to this work.

*Email: nathan.gianneschi@northwestern.edu; nabbott@cornell.edu

Table of Contents

1. Abbreviations

LC, liquid crystal; 5CB, 4-cyano-4'pentylbiphenyl; BODIPY, dipyrromethene boron difluoride; CTA, chain transfer agent; CAC, critical aggregation concentration; RAFT, reversible addition fragmentation chain transfer; DP, degree of polymerization; *Đ*, dispersity; C4, butyl acrylate; C6, hexyl acrylate; C12, dodecyl acrylate; HEA, 2-hydroxyethyl acrylate; DMA, dimethylacrylamide; HEMA, 2-hydroxyethyl methacrylate; AnMA, 9-anthracenylmethyl methacrylate; SEM, scanning electron microscopy; AFM, atomic force microscopy.

2. Characterization methods

^{1}H Nuclear Magnetic Resonance (^{1}H NMR): ^{1}H NMR spectra were recorded on a Varian Inova spectrometer (500 MHz) or a Bruker Avance III HD system equipped with a TXO Prodigy probe (500 MHz) in DMSO-d_6, methanol-d_4, or $CDCl_3$. Chemical shifts are given in ppm downfield from tetramethylsilane TMS.

^{13}C Nuclear Magnetic Resonance (^{13}C NMR): ^{13}C NMR spectra were recorded on a Bruker Avance III 500 MHz system equipped with DCH CryoProbe in $CDCl_3$.

^{11}B Nuclear Magnetic Resonance (^{11}B NMR): ^{11}B NMR spectra were recorded on a Bruker Avance III HD system equipped with a TXO Prodigy probe (500 MHz) in $CDCl_3$.

^{19}F Nuclear Magnetic Resonance (^{19}F NMR): ^{19}F NMR spectra were recorded on a Bruker Avance III HD system equipped with a TXO Prodigy probe (500 MHz) in $CDCl_3$

Gel Permeation Chromatography (GPC): GPC measurements were performed on a set of Phenomenex Phenogel 5 μ, 1 K-75 K, 300 × 7.80 mm in series with a Phenomex Phenogel 5 μ, 10 K-1000 K, 300 x 7.80 mm columns with HPLC grade solvents as eluents: dimethylformamide (DMF) with 0.05 M of LiBr at 60°C. Detection consisted of a Wyatt Optilab T-rEX refractive index detector operating at 658 nm and a Wyatt DAWN® HELEOS® II light scattering detector operating at 659 nm. Molecular weights and dispersities were calculated using the Wyatt ASTRA software with polystyrene standard calibration during GPC analysis.

UV-Vis Spectroscopy: UV−Vis spectra were obtained by using a Cary Series 100 UV-Vis spectrophotometer.

3. Experimental details

3.1 Synthesis of BODIPY-labelled CTA

We synthesized BODIPY-labelled dithiocarbamate CTA in two steps according to the literature.[1] Briefly, 2,4-dimethylpyrrole were reacted with 4-(chloromethyl)benzoylchloride in dichloromethane under reflux conditions for 2 hours. Then the reaction was rotavaped. Toluene and dichloromethane were added to dissolve the product followed by adding triethylamine and stirred under room temperature for 30 mins. Boron trifluoride etherate was added at 50˚C heating and stirred for 1.5 hours. The reaction was purified by column chromatography using hexanes and ethyl acetate as the elution solvent (gradient from 14:1 to 6:1 (v/v)). ^{1}H NMR (500 MHz, Chloroform-d) δ 7.53 (d, *J* = 8.0 Hz, 2H), 7.31 (d, *J* = 8.0 Hz, 2H), 5.99 (s, 2H), 4.67 (s, 2H), 2.57 (s, 6H), 1.39 (s, 6H). UV-Vis (dichloromethane), λ_{max}= 502 nm. After obtaining the BODIPY intermediate, pyrrole was added dropwise to sodium hydride in DMSO and stirred under room temperature for 30 mins. Carbon disulfide was added followed by stirring for 30 mins. Then the BODIPY intermediate was added to the reaction and heated at 50˚C overnight. Afterwards, the reaction was extracted with chloroform for three times, and dried over magnesium sulfate and purified by silica gel column. A mixture of hexanes and dichloromethane was used as the elution solvent (gradient from 2:1 to 1:1 (v/v)). The BODIPY-CTA 1 was obtained as orange powder with 49% yield over three steps.

^{1}H NMR (499 MHz, Chloroform-d) δ 7.73 (t, *J* = 2.3 Hz, 2H), 7.53 (d, *J* = 8.0 Hz, 2H), 7.26 (d, *J* = 8.0 Hz, 2H), 6.41 – 6.32 (t, *J* = 2.3 Hz, 2H), 5.98 (s, 2H), 4.69 (s, 2H), 2.55 (s, 6H), 1.38 (s, 6H). ^{13}C NMR (126 MHz, Chloroform-d) δ 198.79, 155.63, 143.03, 141.01, 135.80, 134.64, 131.35, 130.04, 128.43, 121.31, 120.74, 114.38, 41.14, 14.61, 14.50. ^{19}F NMR (470 MHz, Chloroform-d) δ -146.32 (q, *J* = 32.9 Hz). ^{11}B NMR (160 MHz, Chloroform-d) δ 0.76 (t, *J* = 33.0 Hz). UV-Vis (dichloromethane), λ_{max}= 502 nm. MS (ESI^{+}): Calculated for $C_{25}H_{25}BF_2N_3S_2^{+}$ $[M+H]^{+}$: 480.16, found: 480.22.

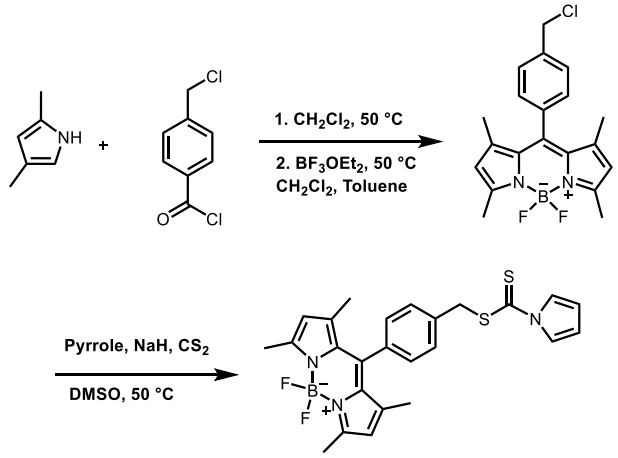

Figure S1. Synthetic route for BODIPY-CTA 1.

To match the reactivity of methacrylate monomers, a trithiocarbonate CTA (BODIPY-CTA 2) was synthesized by esterification of a phenol BODIPY with a -COOH bearing trithiolcarbonate (**Figure S2**). 4-Cyano-4-[(dodecylsulfanylthiocarbonyl)sulfanyl]pentanoic acid (CTA 2) was reacted with N-Hydroxysuccinimide (NHS) to form the NHS activated ester, and then reacted with the BODIPY phenol under N,N-Diisopropylethylamine in dichloromethane. The reaction was purified by silica gel column using a hexanes/ethyl acetate solvent system (gradient from 12:1, 10:1 to 8:1 (v/v)). There is 10% unreacted starting material in the 2, as shown in the ^{1}H NMR.

^{1}H NMR (500 MHz, Chloroform-d) δ 7.34 (d, *J* = 8.5 Hz, 2H), 7.27 (d, *J* = 8.5 Hz, 2H), 6.01 (s, 2H), 3.37 (t, *J* = 7.2 Hz, 2H), 2.96 (t, *J* = 7.7 Hz, 2H), 2.76 – 2.63 (m, 2H), 2.58 (s, 6H), 2.56-2.50 (s, 2H), 2.56 – 2.48 (m, 1H), 1.97 (s, 3H), 1.73 (p, *J* = 7.5 Hz, 3H), 1.44 (s, 6H), 1.27 (b, 16H), 0.94 – 0.88 (m, 3H). ^{13}C NMR (126 MHz, Chloroform-d) δ 216.74, 169.75, 155.77, 150.98, 143.06, 140.45, 132.76, 131.42, 129.30, 122.33, 121.42, 118.94, 116.11, 46.31, 37.15, 33.77, 31.92, 30.06, 29.63, 29.55, 29.43, 29.35, 29.08, 28.95, 27.69, 25.08, 22.70, 14.61, 14.55, 14.14. ^{19}F NMR (470 MHz, Chloroform-d) δ -146.28 (t, *J* = 32.9 Hz). ^{11}B NMR (160 MHz, Chloroform-d) δ 0.76. (t, *J* = 33.1 Hz). MS (ESI^{+}): Calculated for $C_{38}H_{50}BF_2N_3NaO_2S_3^{+}$ [M+Na]$^{+}$: 748.30, found: 748.36.

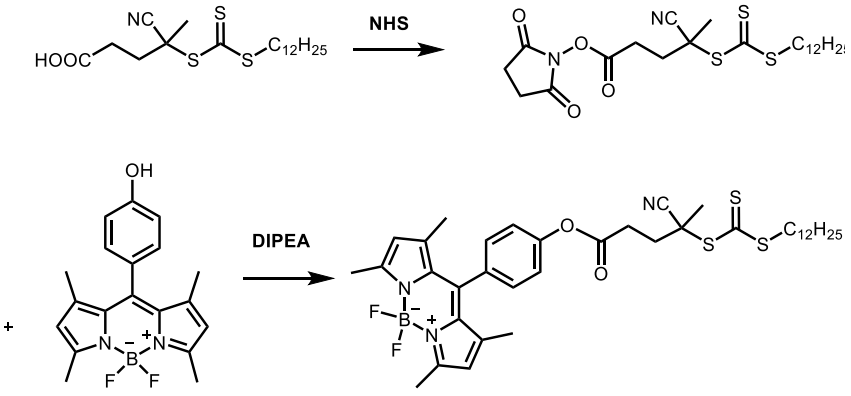

Figure S2. Synthetic route of trithiocarbonate BODIPY-CTA 2.

3.2 Representative synthesis procedure of BODIPY-labelled polymer

RAFT (reversible addition fragmentation transfer) polymerization was performed in DMF with AIBN as the initiator. Typically for BODIPY-poly(C4), the starting materials BODIPY-CTA 1 (4.8 mg, 0.01 mmol), C4 (144 μL, 1 mmol), AIBN (0.8 mg, 0.005 mmol) were added in a flame-dried 10 mL Schlenk flask under nitrogen flow. 0.5 mL DMF were freshly taken from solvent system. The system was subsequently degassed by three freeze-pump-thaw cycles. Then the flask was immersed in a 70℃ oil bath and allowed to react overnight under continues nitrogen flow. The reaction was quenched by immersing in liquid nitrogen and then precipitate three times in cold methanol. Finally, the BODIPY-poly(C4) were collected by centrifuge and dried under vacuum overnight before use. The polymer was characterized by ^{1}H NMR and GPC.

^{1}H NMR (500 MHz, Chloroform-d) δ 4.06 (s, 2H), 2.29 (s, 1H), 1.93 (s, 1H), 1.61 (s, 3H), 1.40 (s, 2H), 0.96 (t, J = 7.4 Hz, 3H). GPC (in THF), M_n = 12.9 kg/mol, $Đ$ =1.17.

For the precipitation procedure, hexanes or diethyl ether were also used depending on the solubility of the polymer. Non-polar polymers include C4, C6 and C12. Polar polymers are HEMA, HEA and DMA. Cross-linkable polymers were made by copolymerization methods.

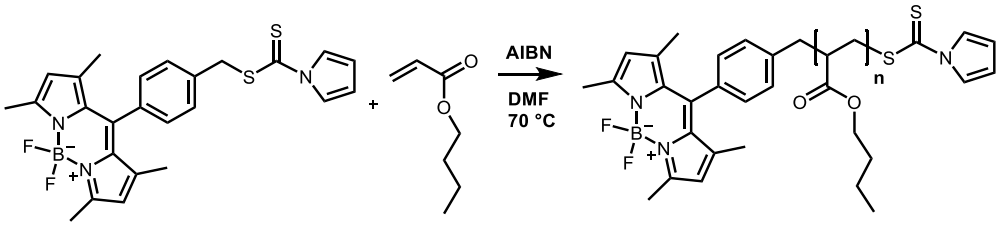

Figure S3. Synthetic route for BODIPY-poly(C4).

4. Characterization of BODIPY CTA

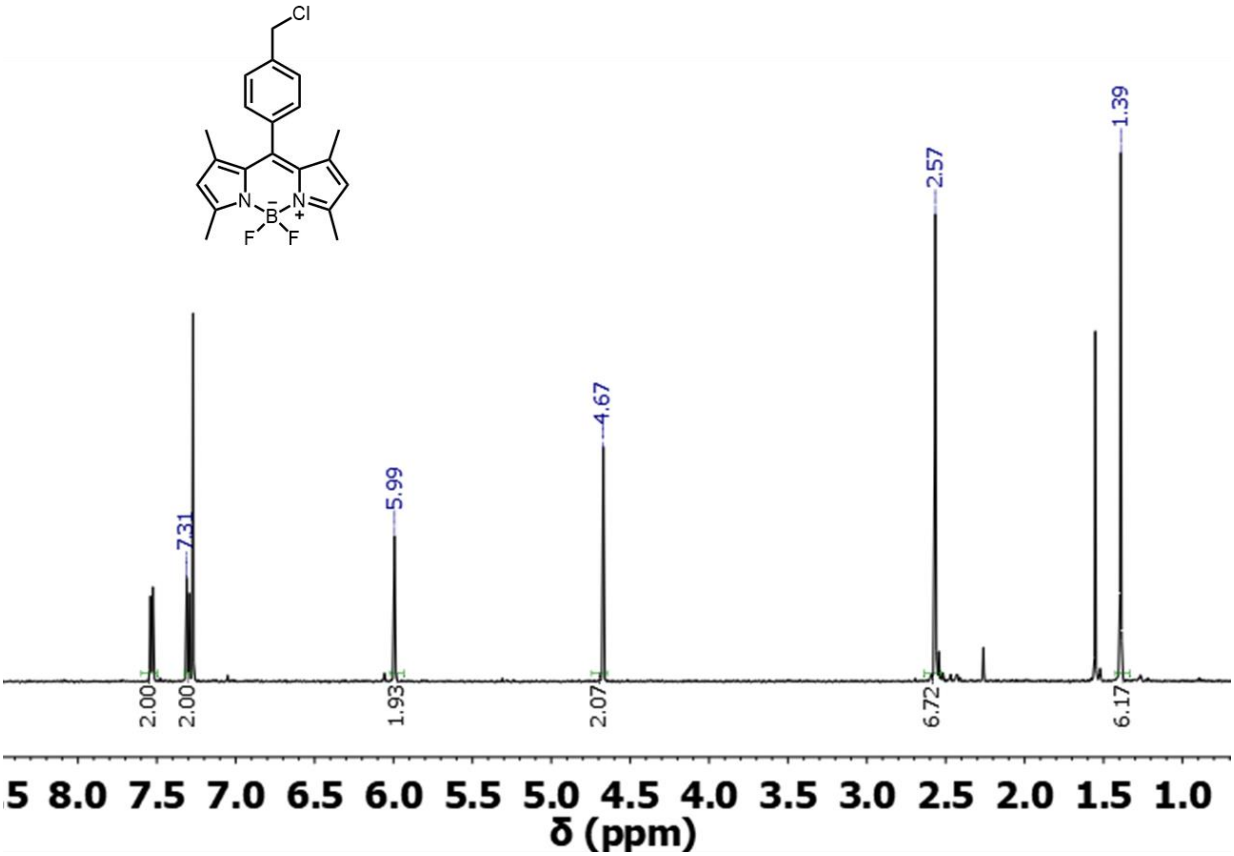

Figure S4. ^{1}H NMR of BODIPY intermediate.

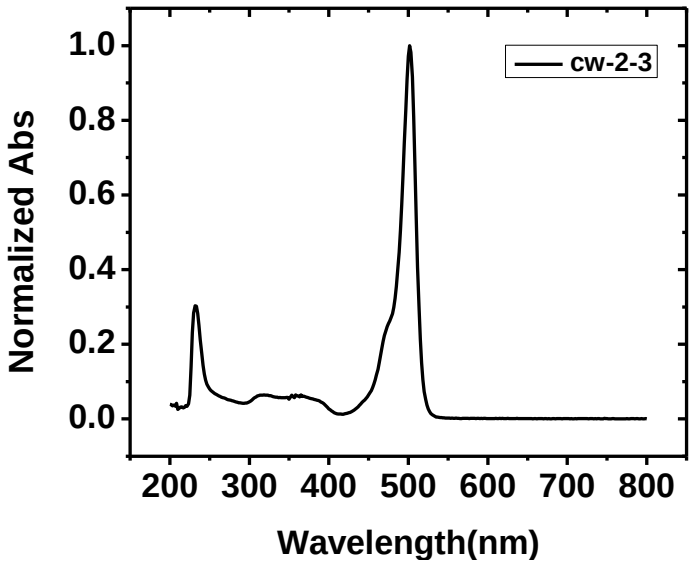

Figure S5. UV-vis spectrum of BODIPY intermediate in dichloromethane.

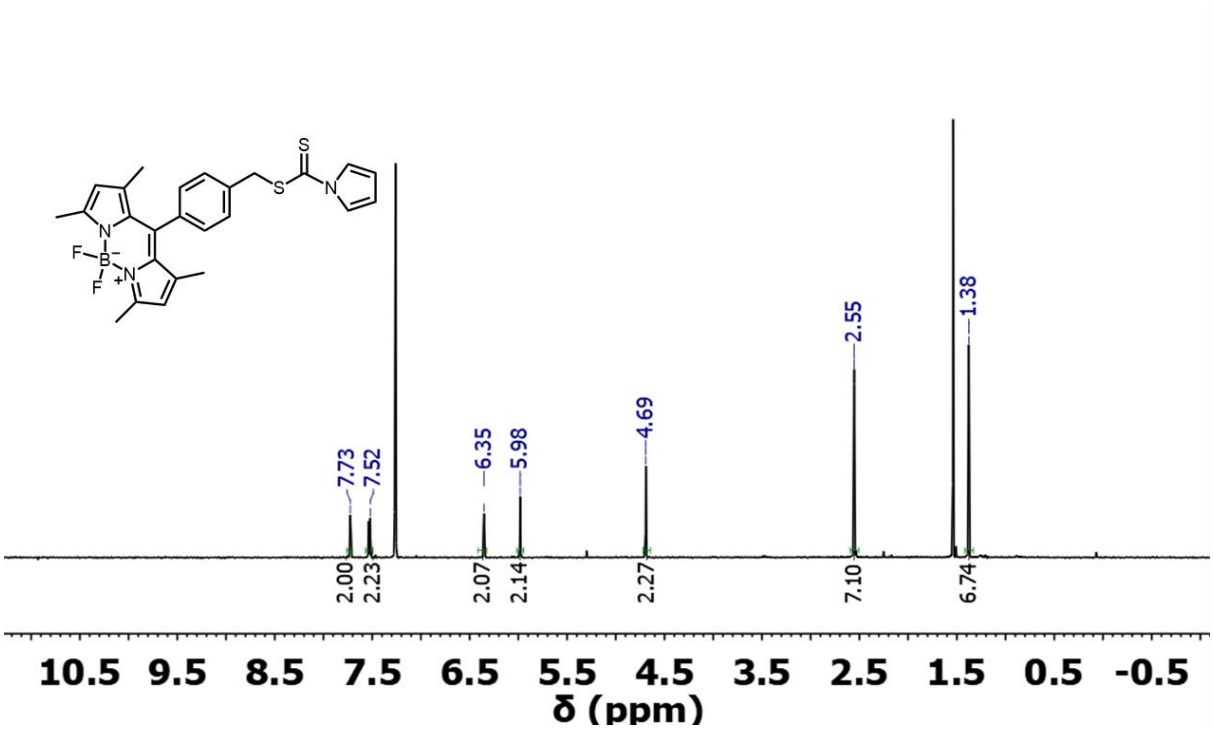

Figure S6. ^{1}H NMR of BODIPY-CTA 1.

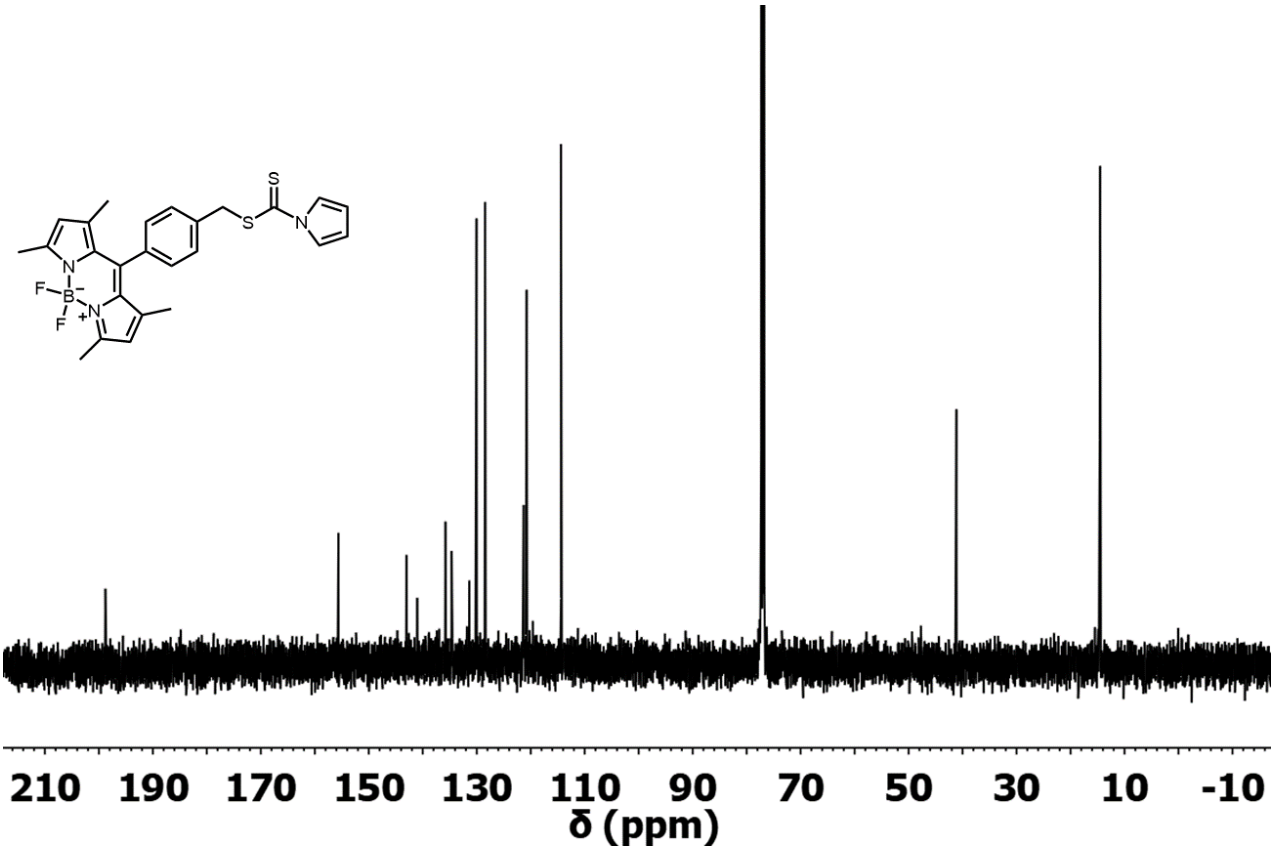

Figure S7. ^{13}C NMR of BODIPY-CTA 1.

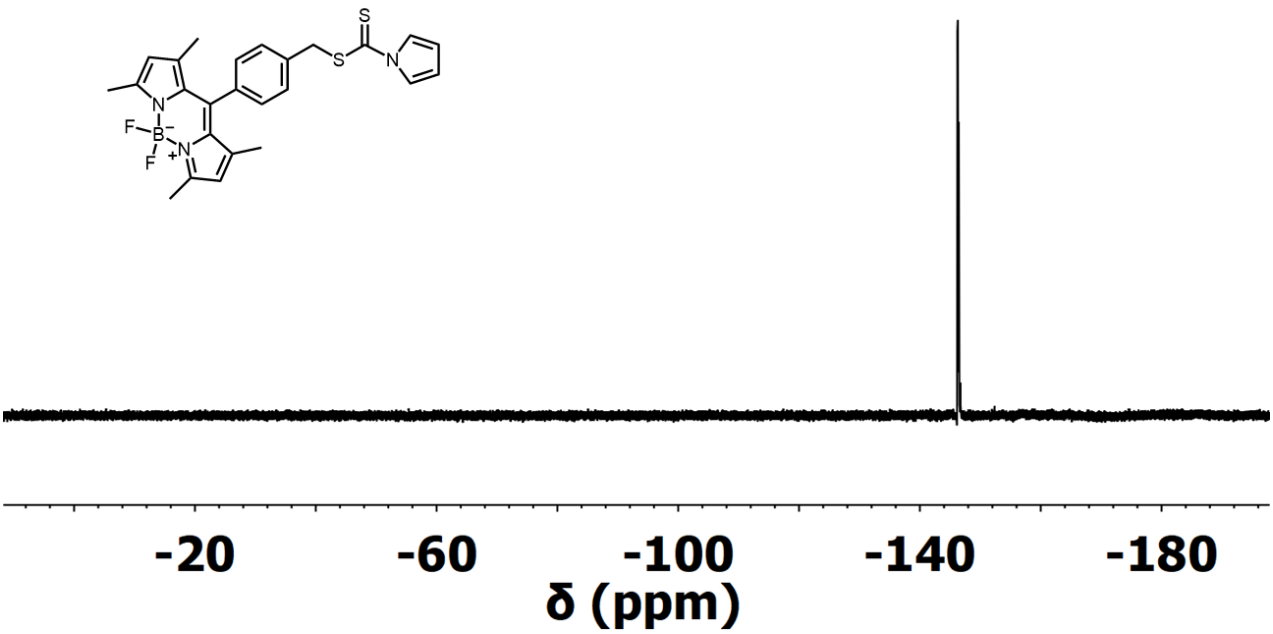

Figure S8. ^{19}F NMR of BODIPY-CTA 1.

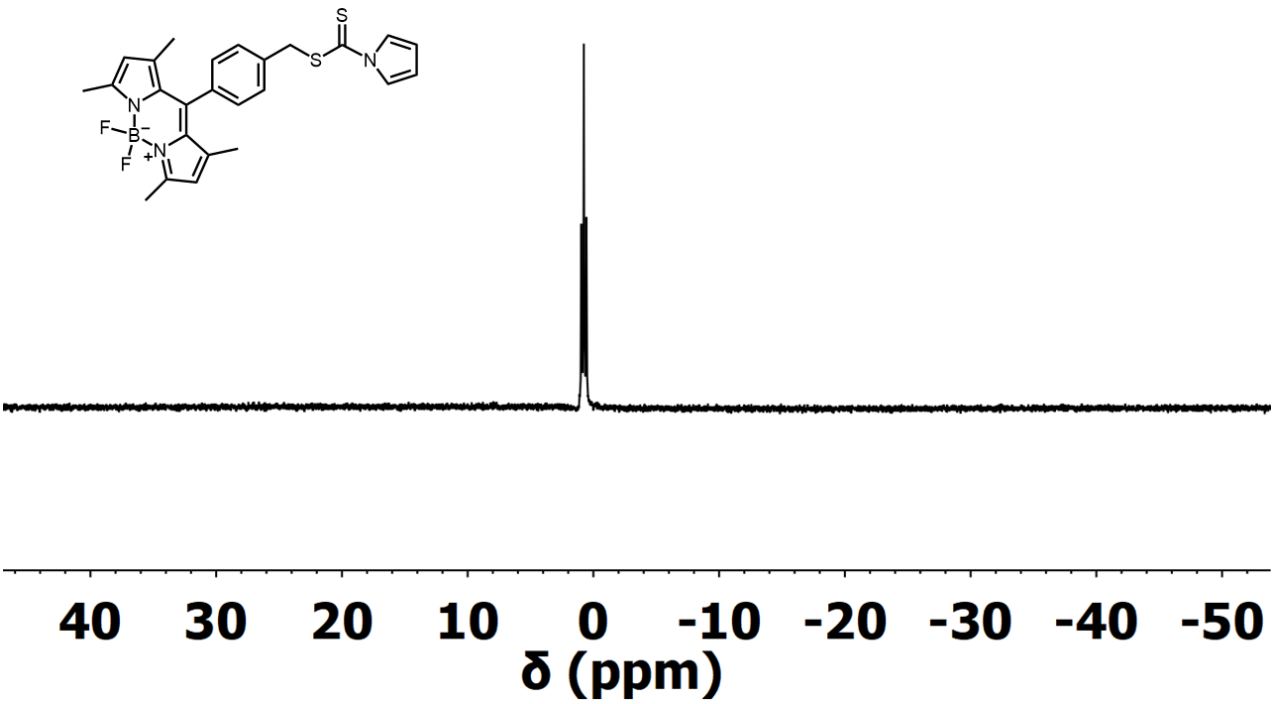

Figure S9. ^{11}B NMR of BODIPY-CTA 1.

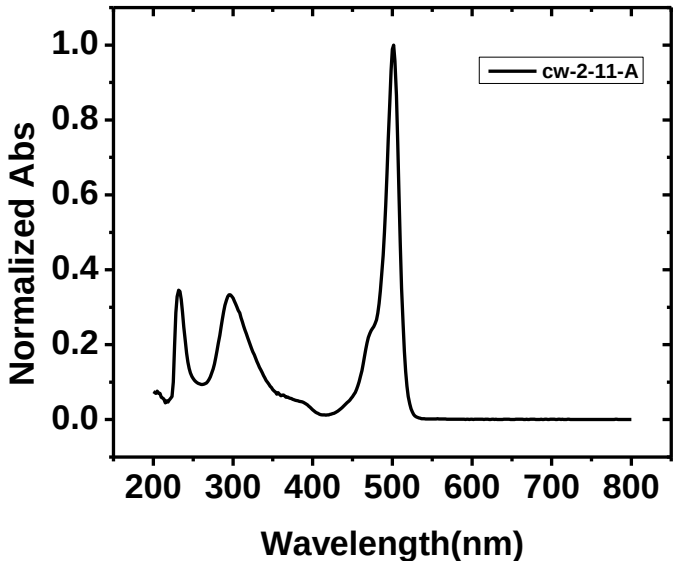

Figure S10. UV-Vis spectrum of BODIPY-CTA 1 in dichloromethane.

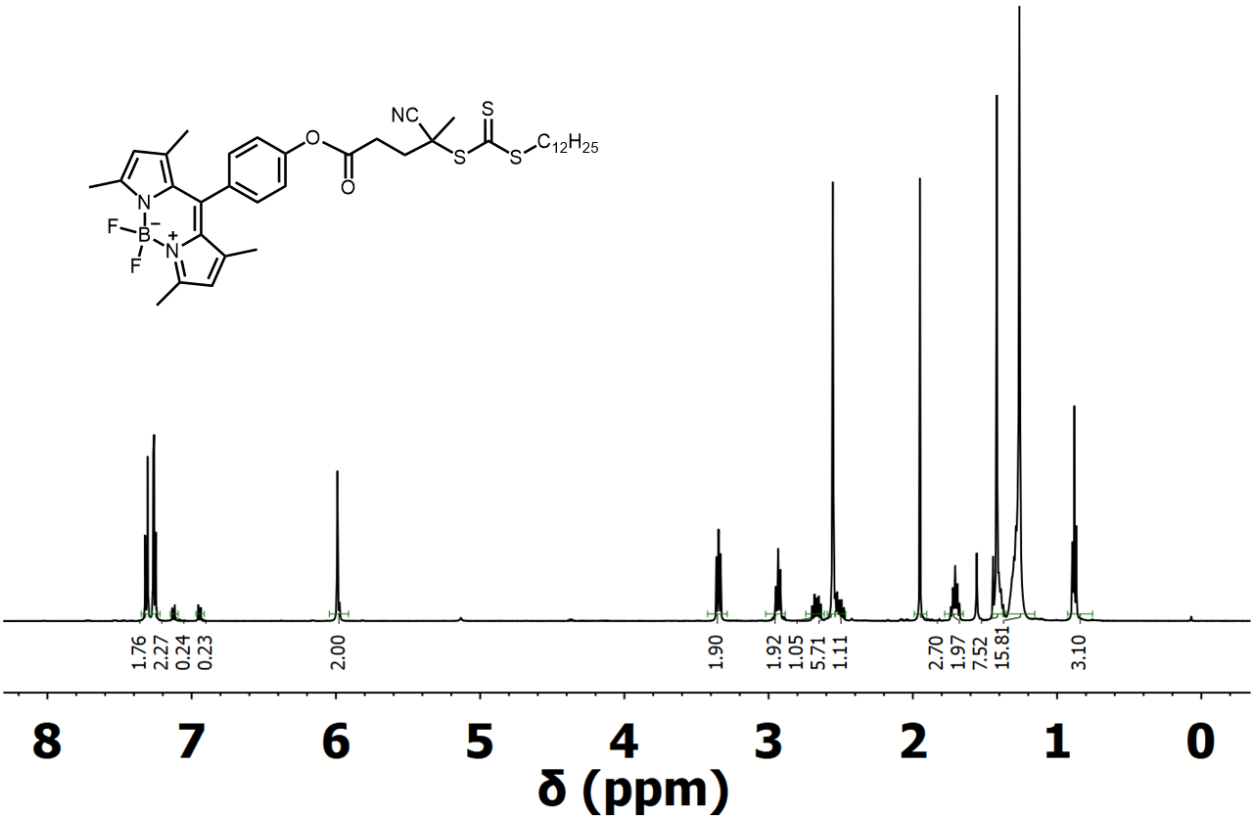

Figure S11. ^{1}H NMR of BODIPY-CTA 2.

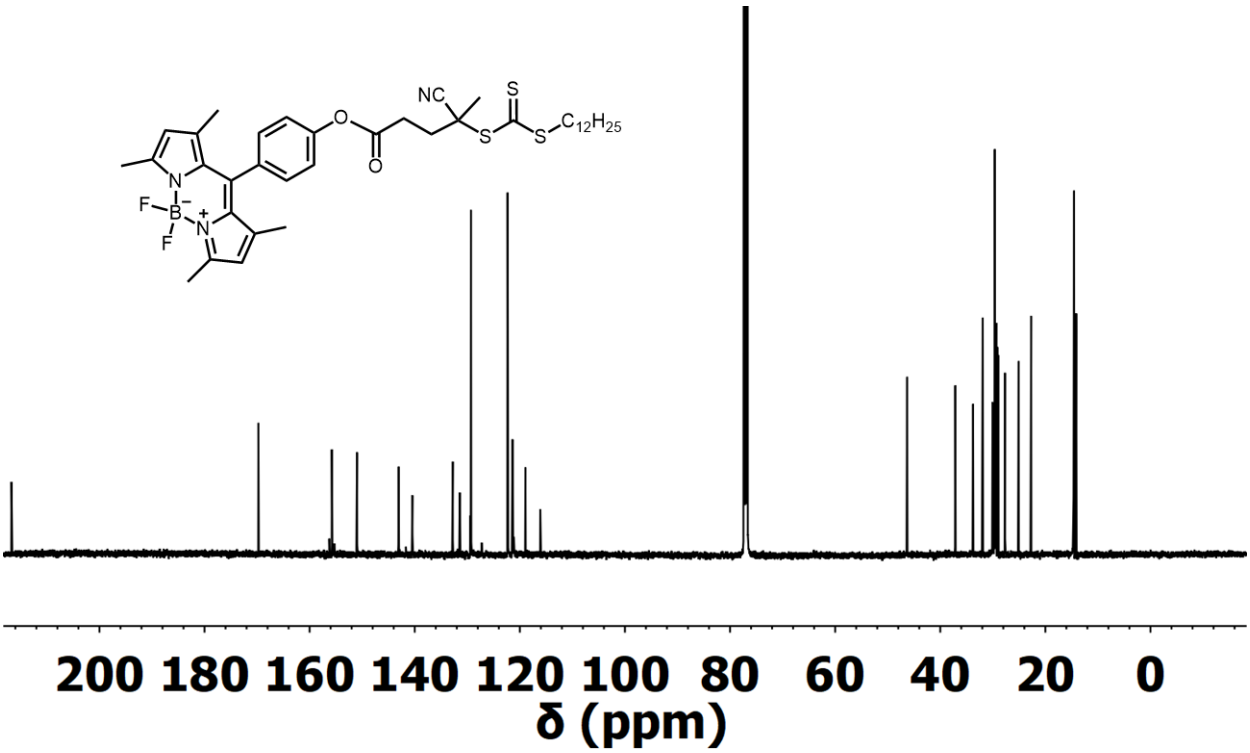

Figure S12. ^{13}C NMR of BODIPY-CTA 2.

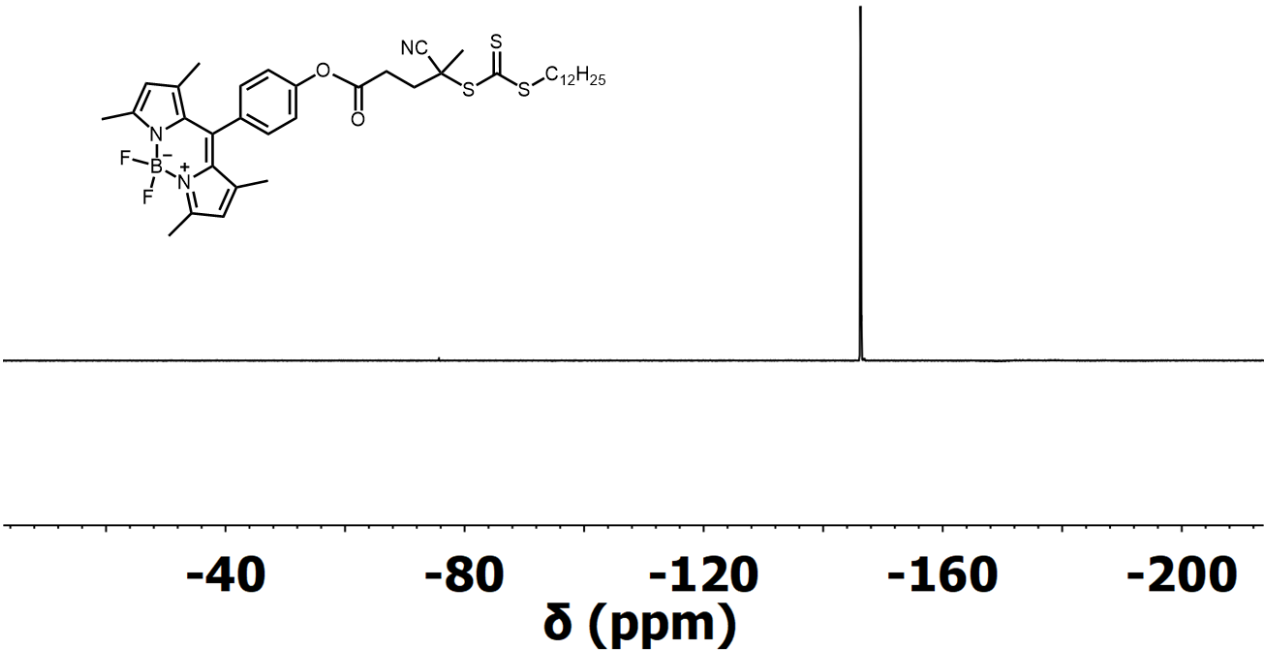

Figure S13. ^{19}F NMR of BODIPY-CTA 2.

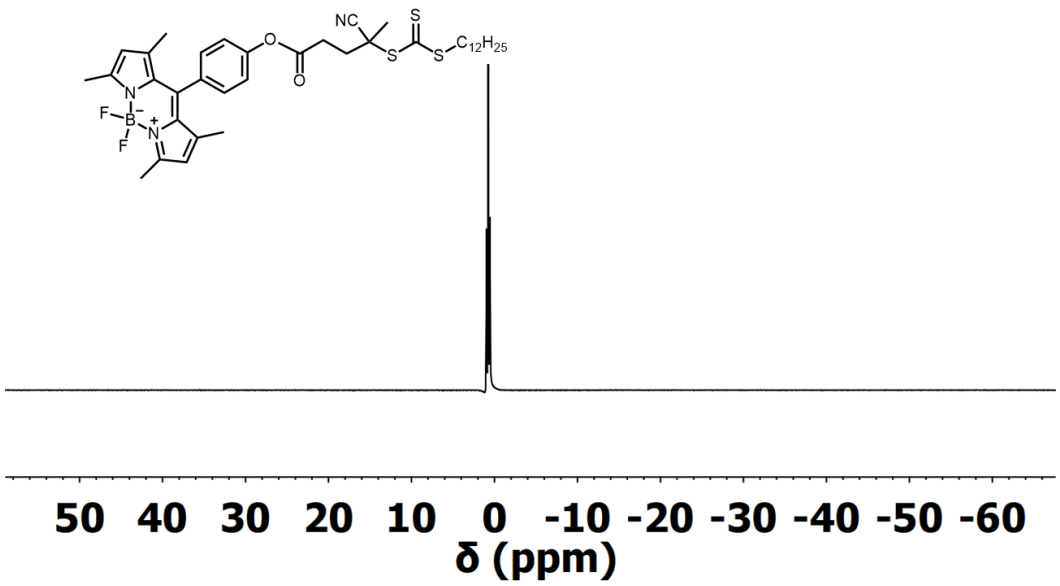

Figure S14. ^{11}B NMR of BODIPY-CTA 2.

5. Characterization of BODIPY-labelled polymers

5.1 Characterization of BODIPY-poly(C4)

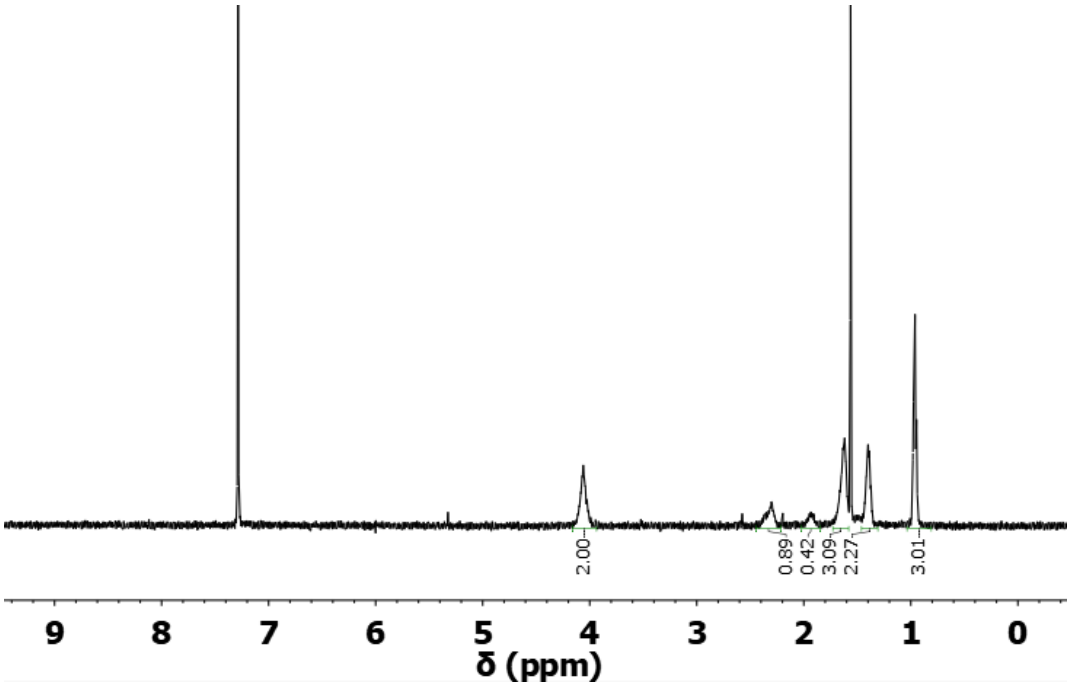

Figure S15. ^{1}H NMR of BODIPY-poly(C4) (DP = 103).

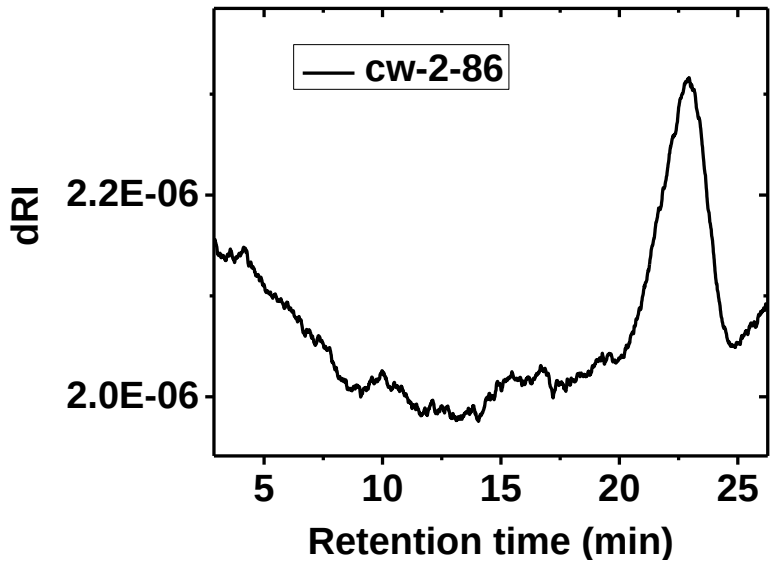

Figure S16. GPC plot of BODIPY-poly(C4) (DP = 103).

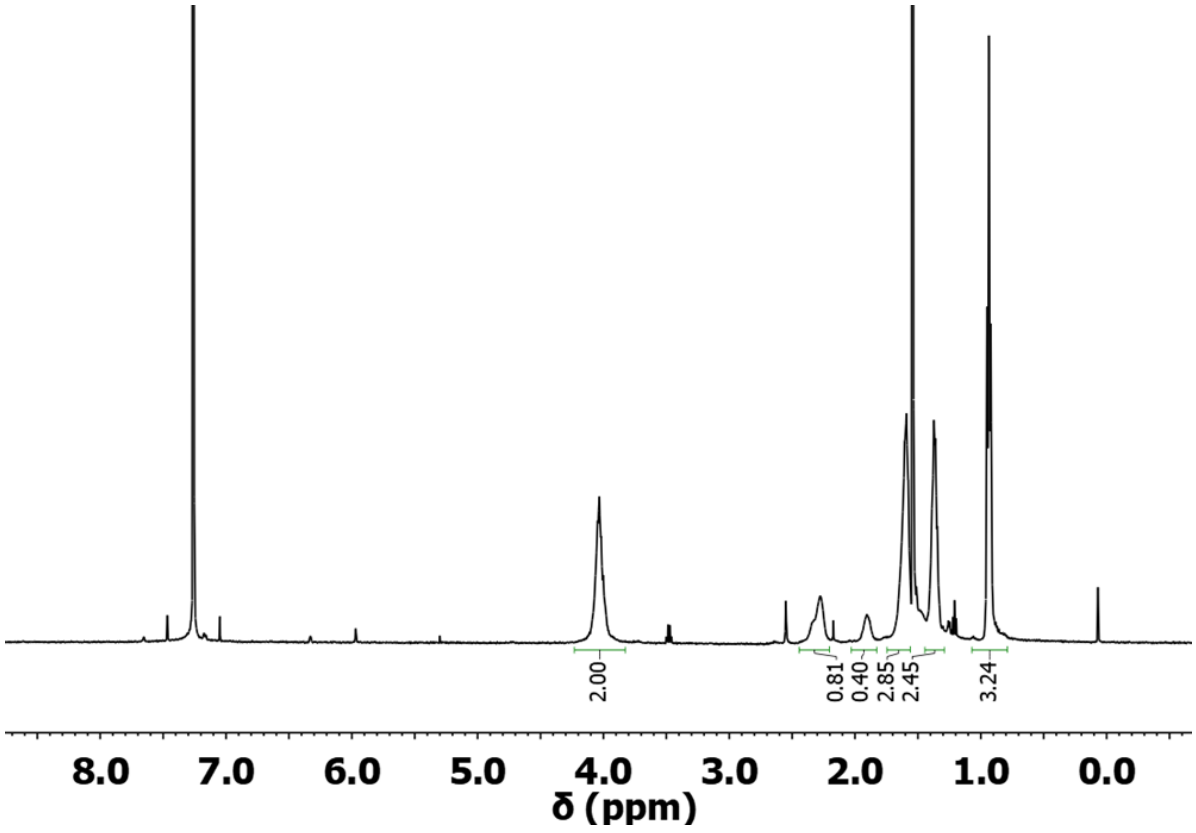

Figure S17. ^{1}H NMR of BODIPY-poly(C4) (DP = 50).

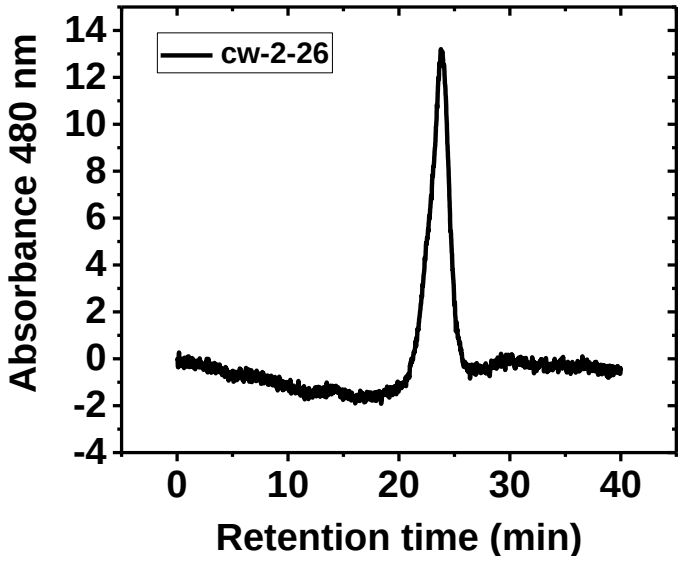

Figure S18. GPC trace of BODIPY-poly(C4) (DP = 50).

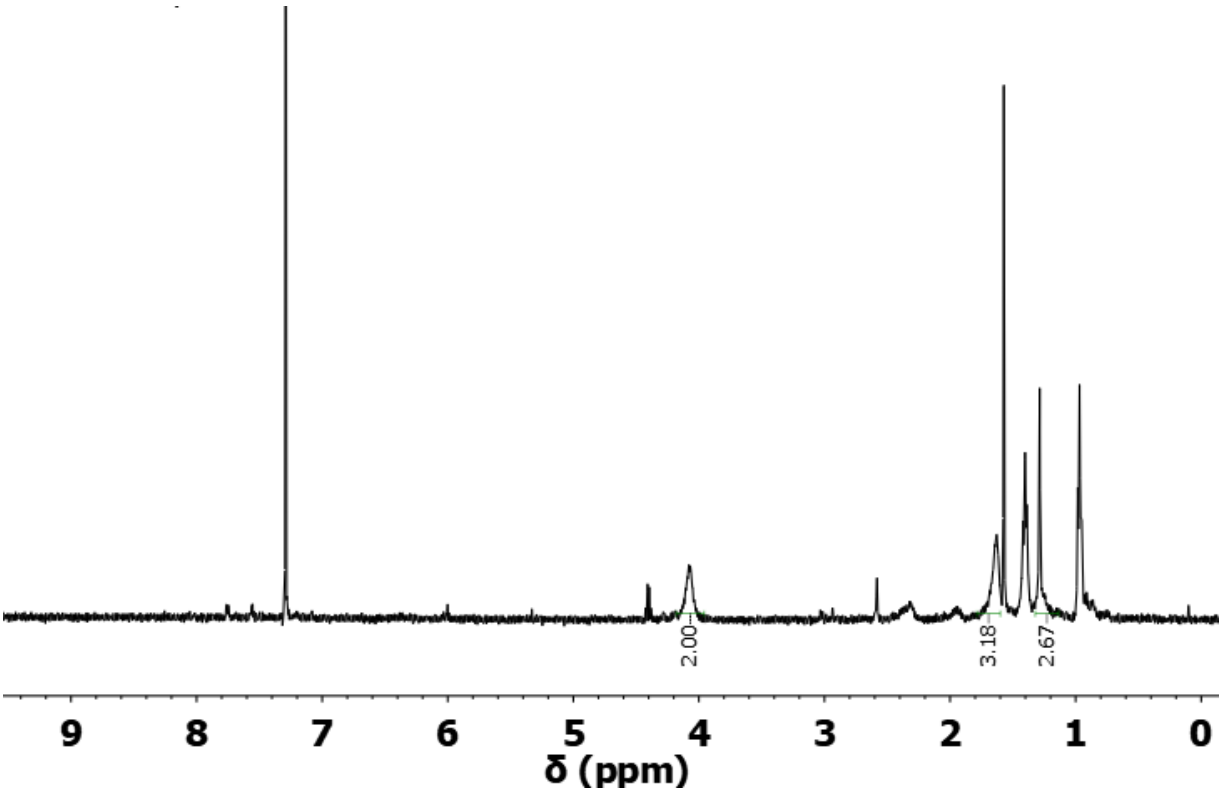

Figure S19 ^{1}H NMR of BODIPY-poly(C4) (DP = 14). The molecular weight of this polymer is too small (elution time too long) to be measured by GPC.

5.2 Characterization of BODIPY-poly(C6)

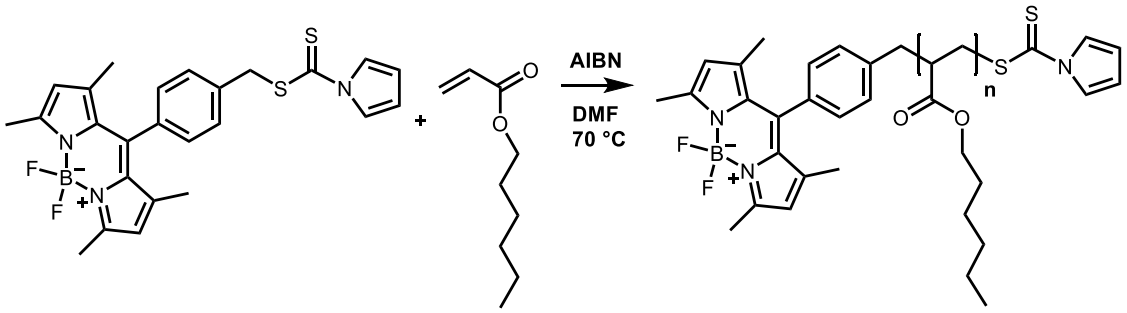

Figure S20. Synthetic route for BODIPY-poly(C6).

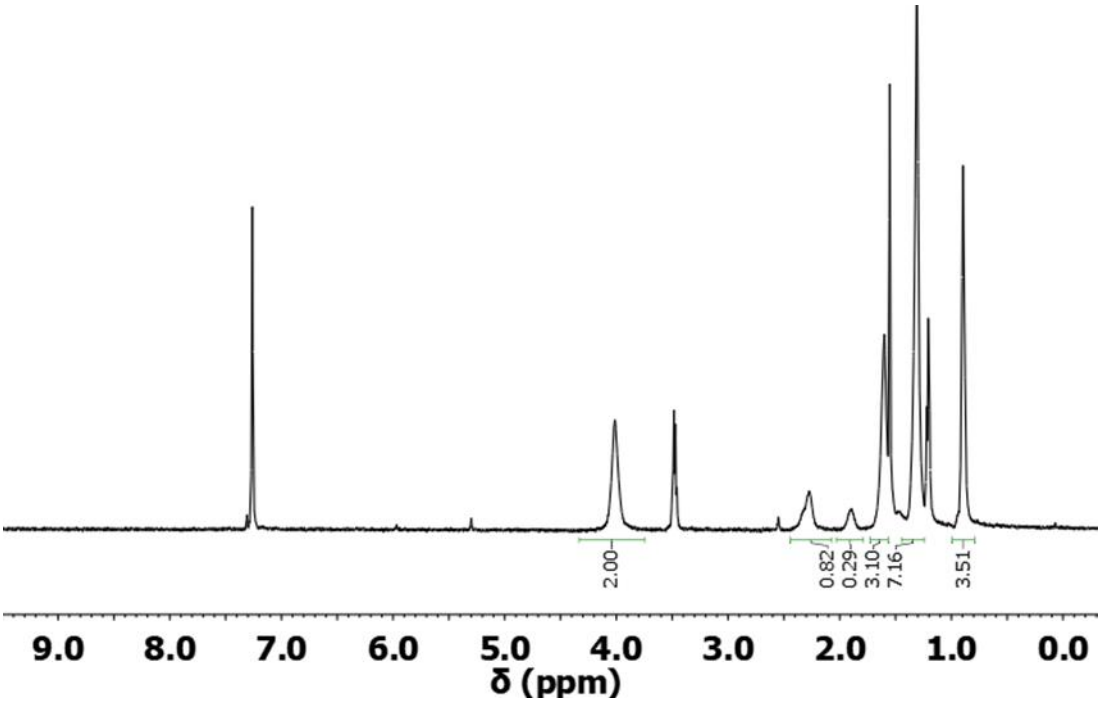

Figure S21. ^{1}H NMR of BODIPY-poly(C6) (DP = 72).

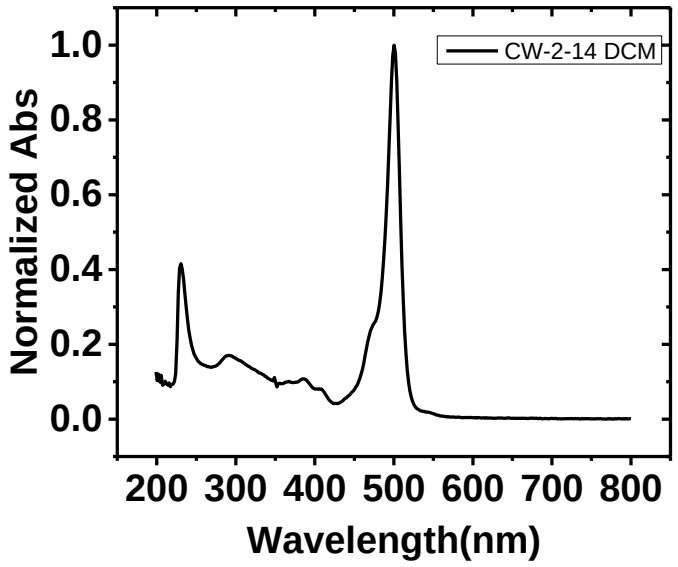

Figure S22. UV-Vis spectrum of BODIPY-poly(C6) (DP = 72) in dichloromethane.

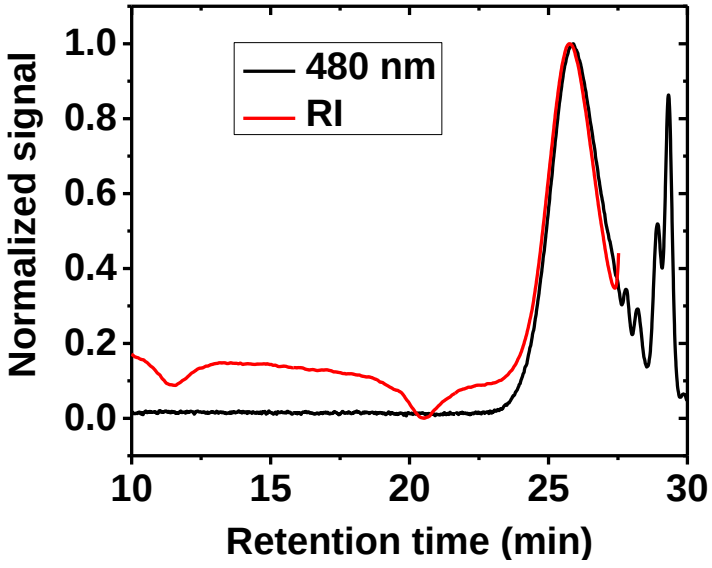

Figure S23. GPC plot of BODIPY-poly(C6) (DP = 72). THF as the eluent.

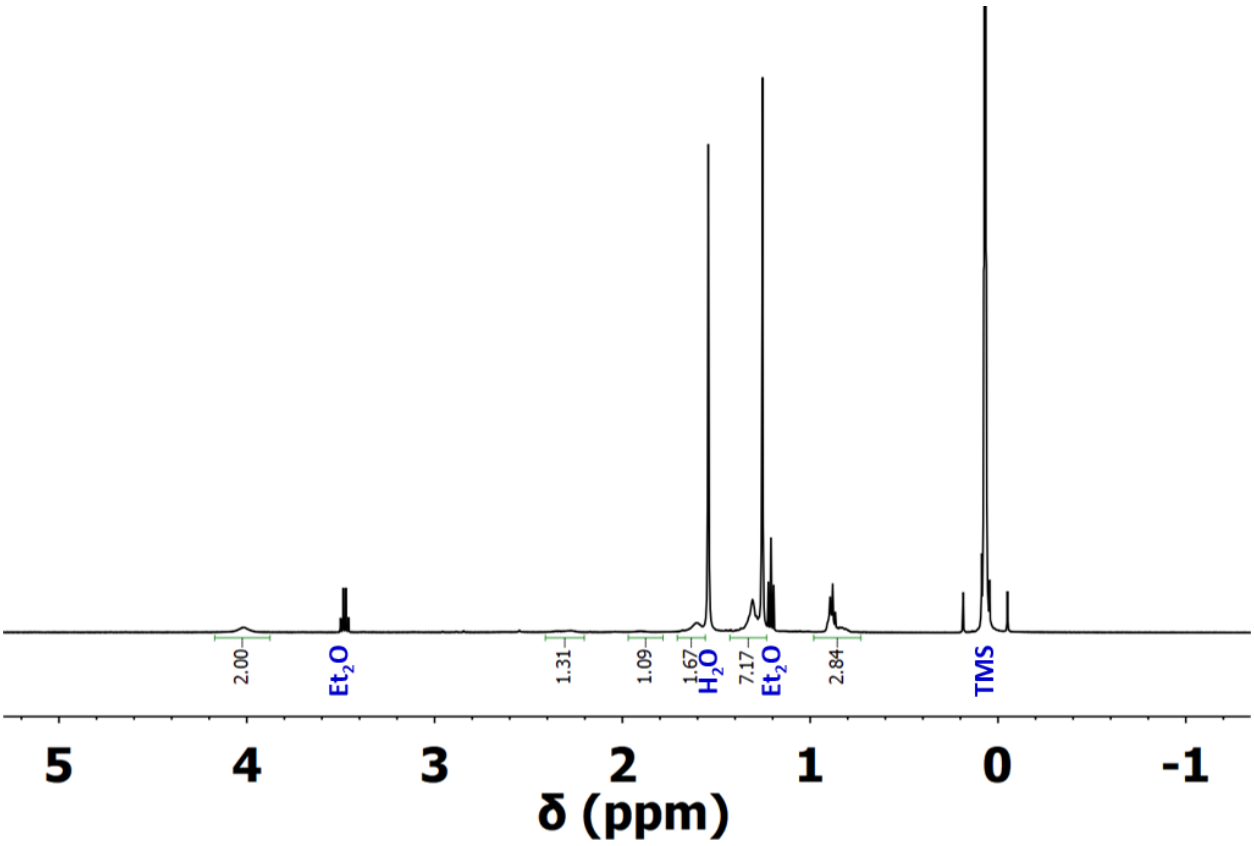

Figure S24. ^{1}H NMR of BODIPY-poly(C6) (DP = 18).

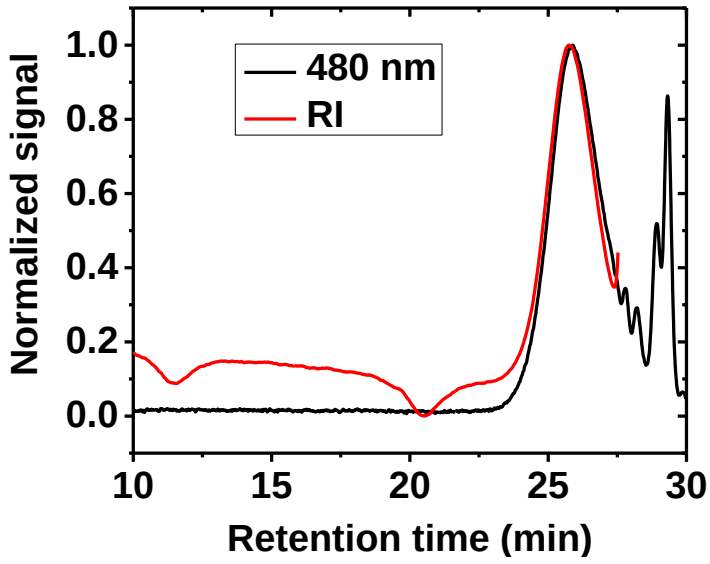

Figure S25. GPC plot of BODIPY-poly(C6) (DP = 18). THF as the eluent.

5.3 Characterization of BODIPY-poly(C12)

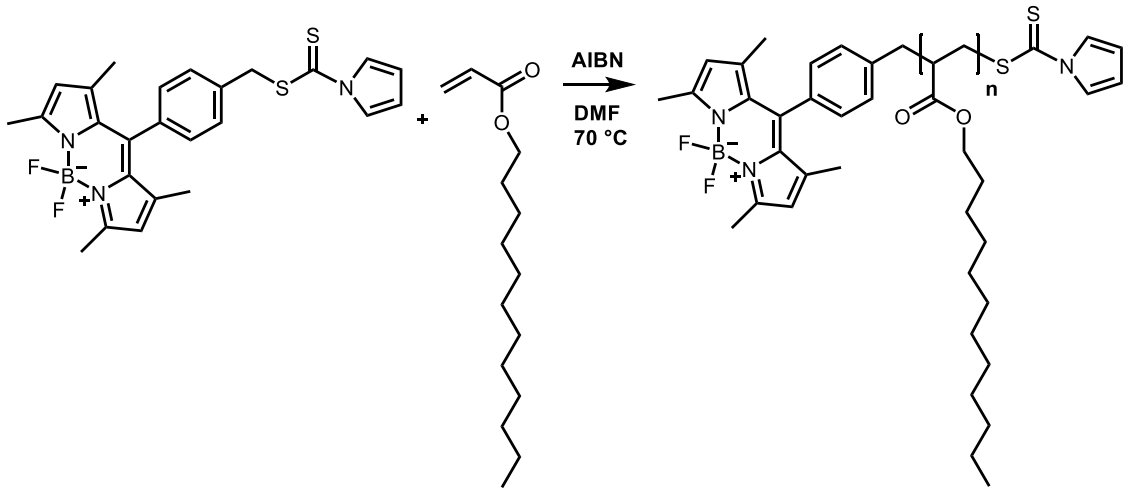

Figure S26. Synthetic route for BODIPY-poly(C12).

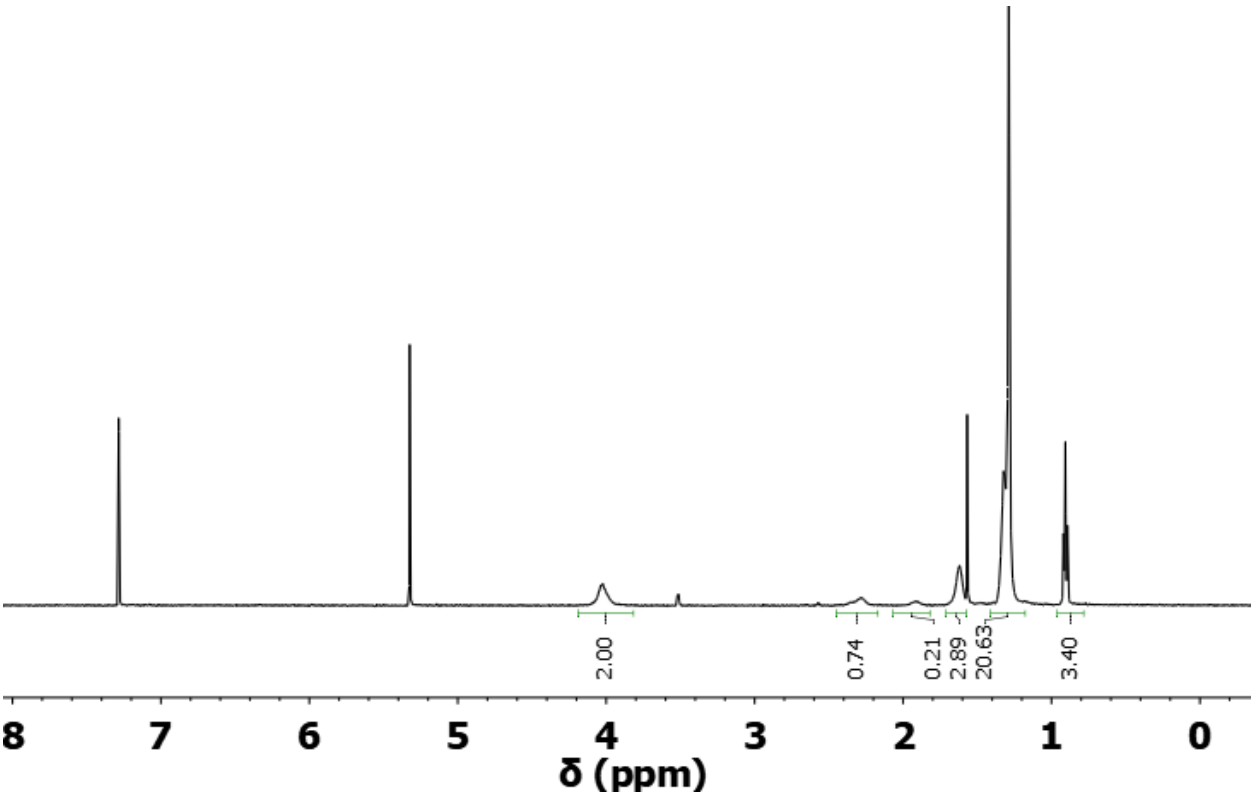

Figure S27. ^{1}H NMR of BODIPY-poly(C12) (DP = 107).

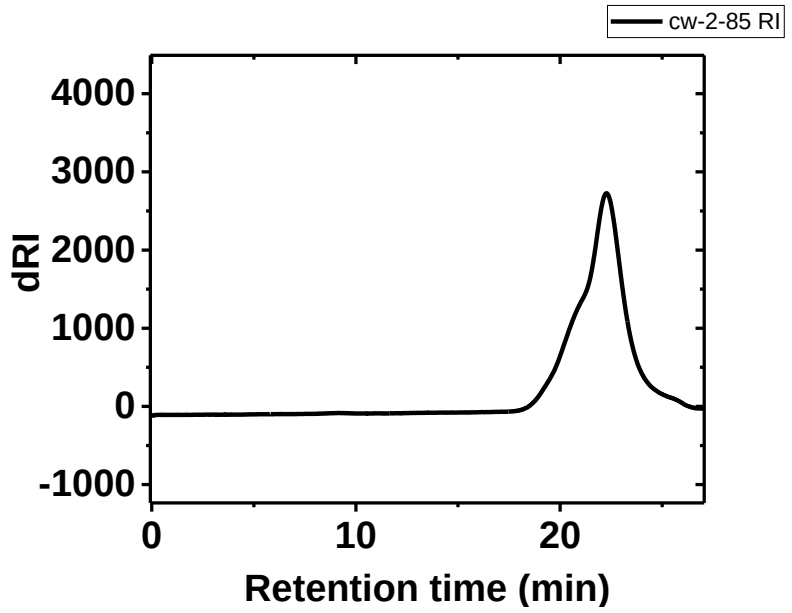

Figure S28. GPC plot of BODIPY-poly(C12) (DP = 107). THF as the eluent.

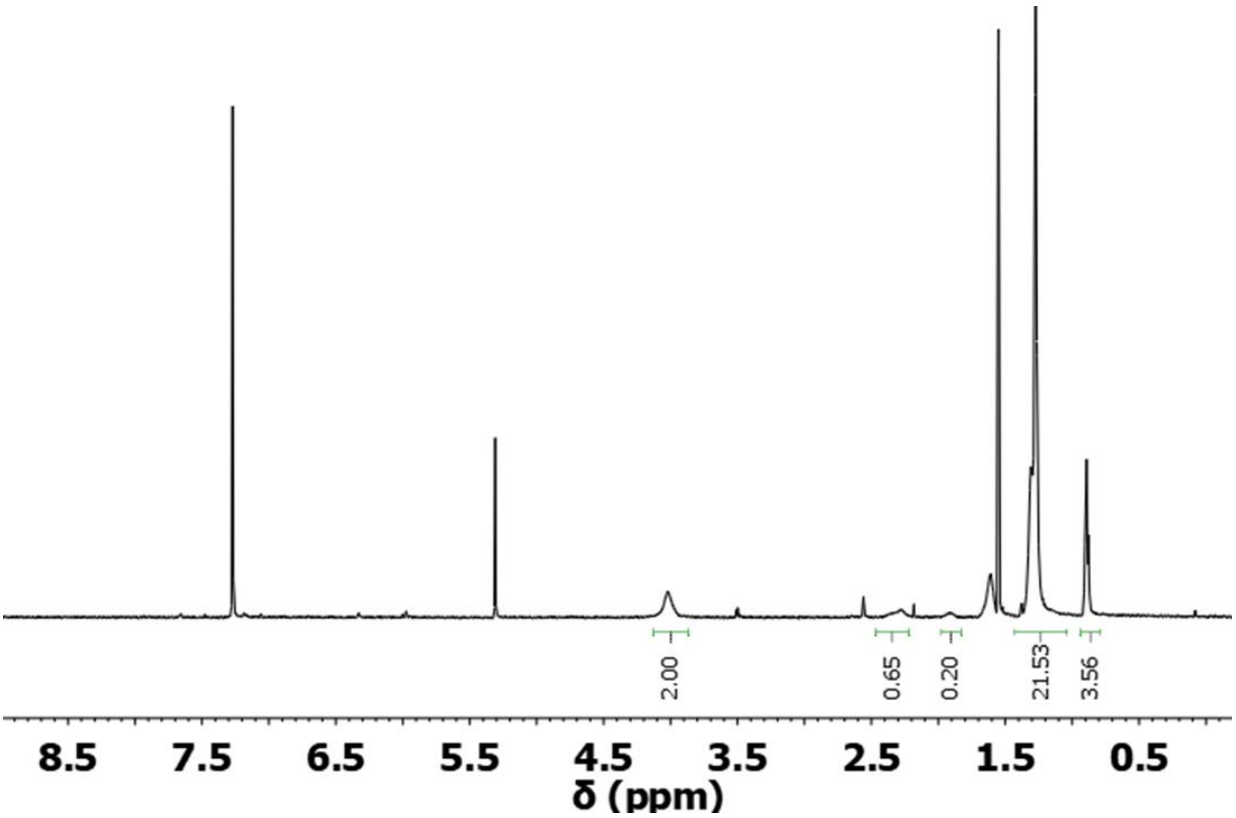

Figure S29. ^{1}H NMR of BODIPY-poly(C12) (DP = 39).

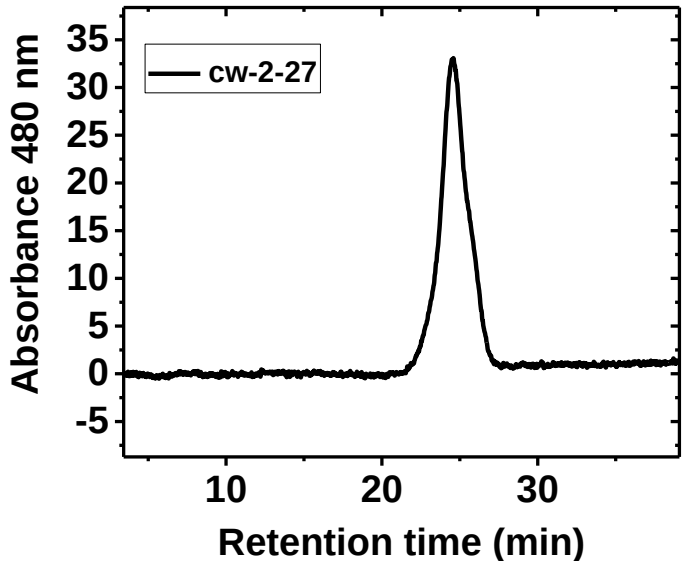

Figure S30. GPC plot of BODIPY-poly(C12) (DP = 39)

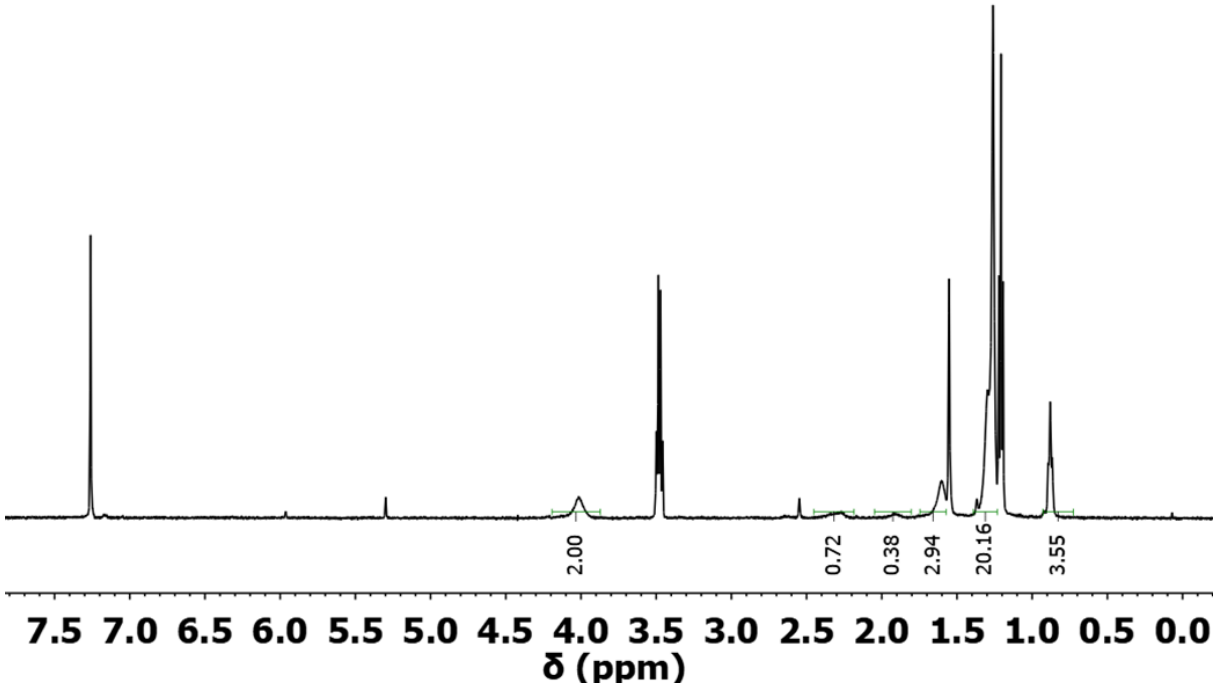

Figure S31. ^{1}H NMR of BODIPY-poly(C12) (DP = 5).

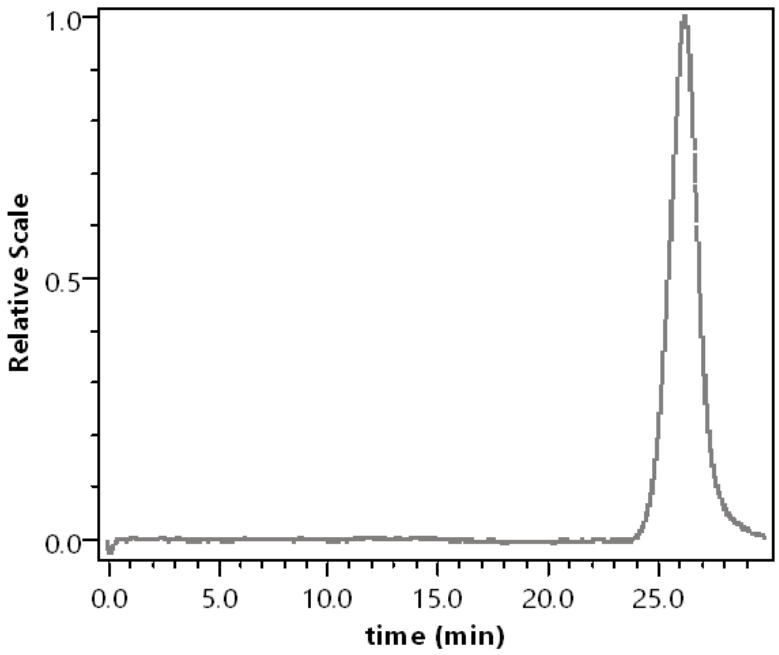

Figure S32. GPC plot of BODIPY-poly(C12) (DP = 5). The molecular weight of this polymer is too small to be measured by GPC.

5.4 Characterization of BODIPY-poly(DMA)

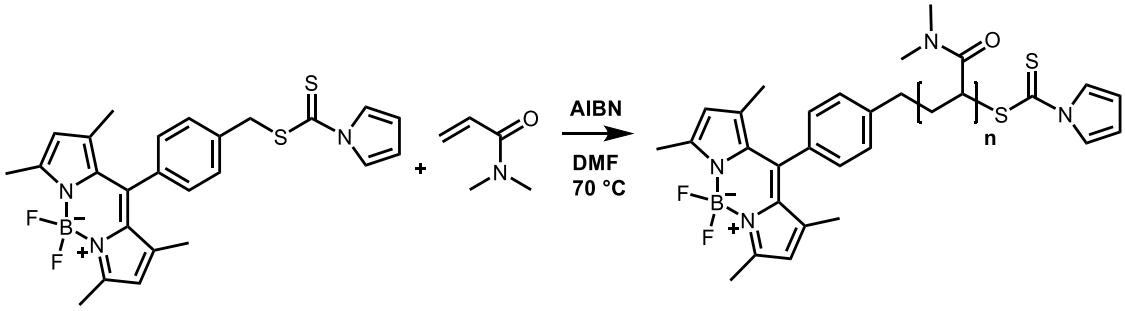

Figure S33. Synthetic route of BODIPY-poly(DMA).

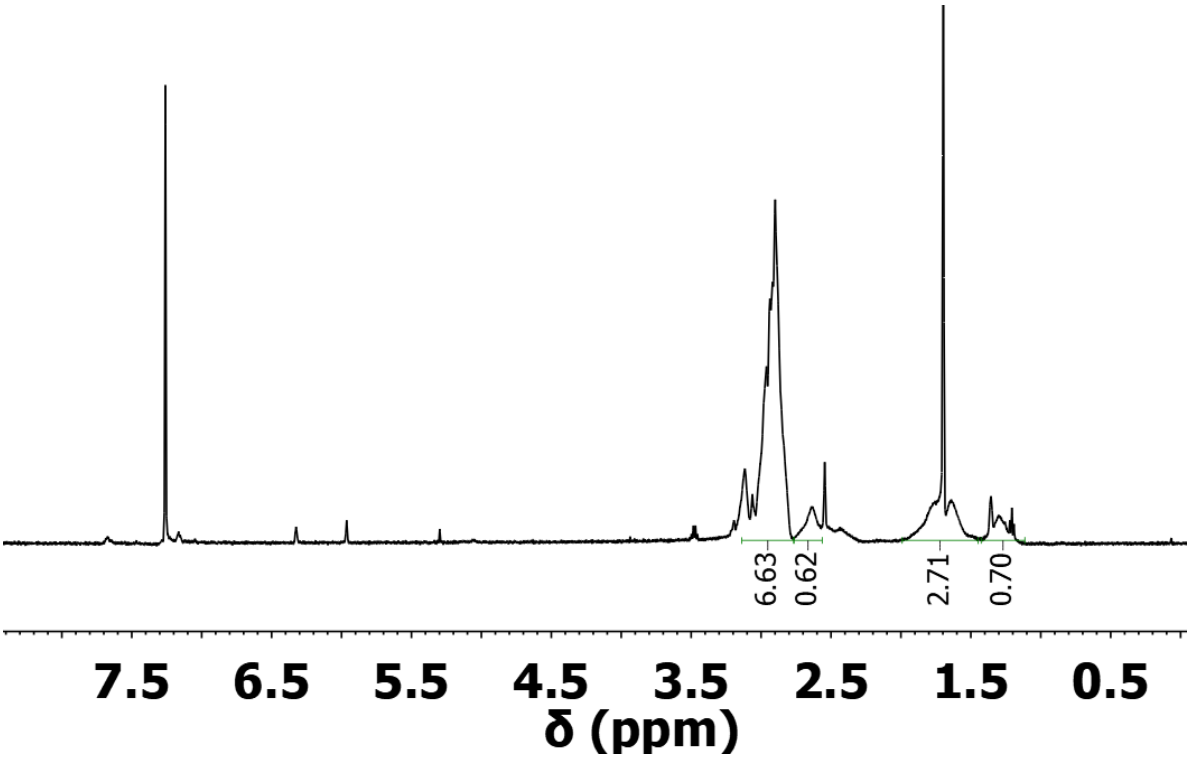

Figure S34. ^{1}H NMR of BODIPY-poly(DMA) (DP = 32).

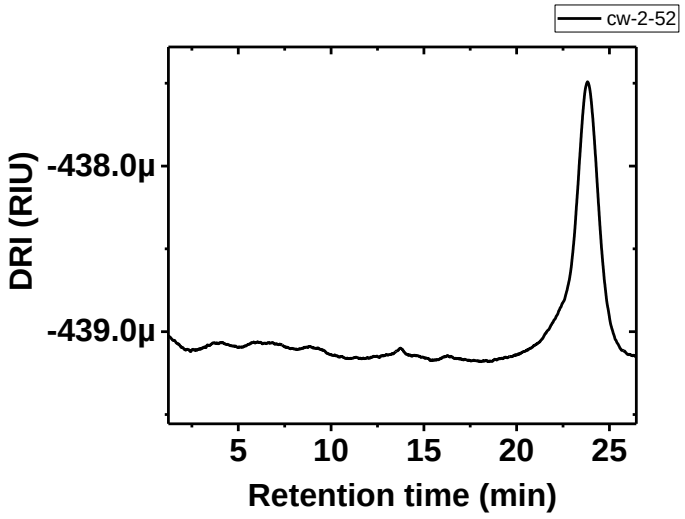

Figure S35. GPC plot of BODIPY-poly(DMA) (DP = 32).

5.5 Characterization of the BODIPY-poly(HEA)

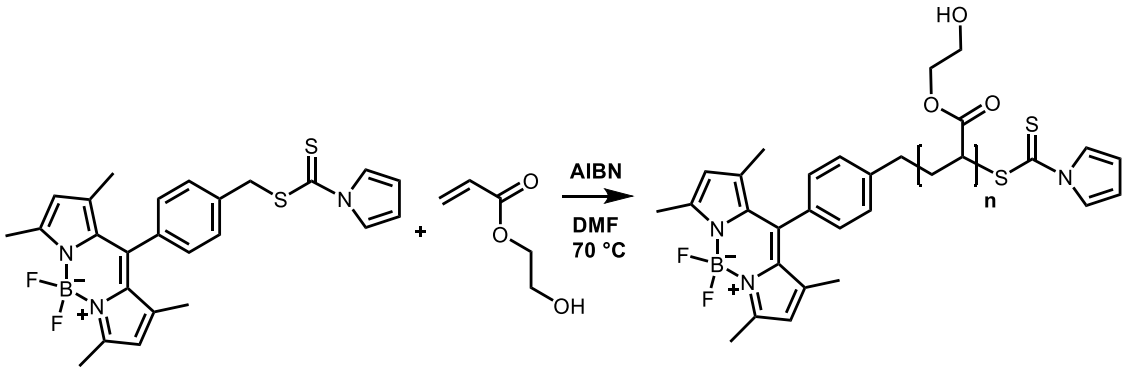

Figure S36. Synthetic route of BODIPY-poly(HEA).

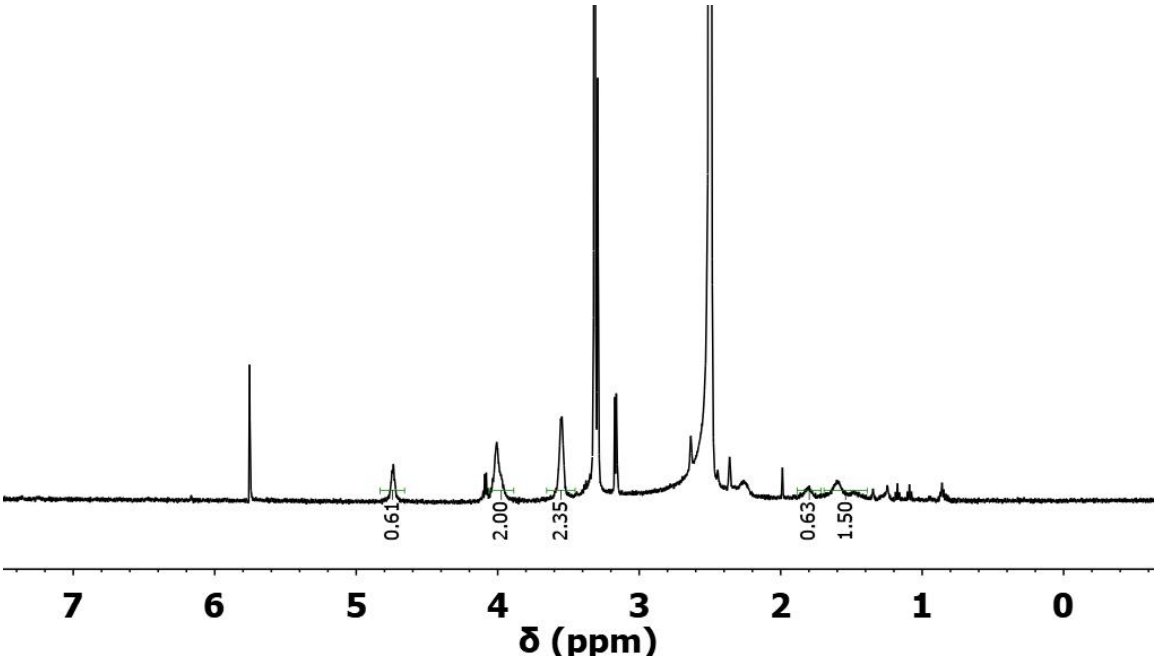

Figure S37. ^{1}H NMR of BODIPY-poly(HEA) (DP = 38).

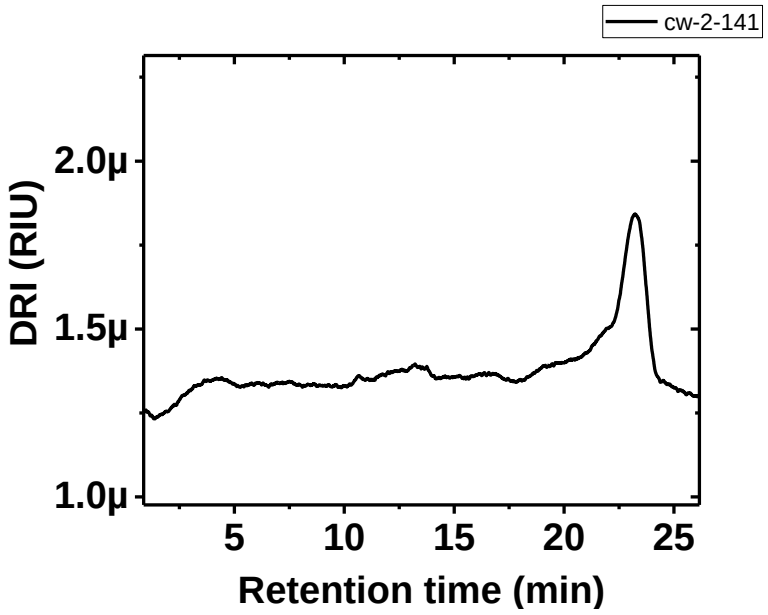

Figure S38. GPC plot of BODIPY-poly(HEA) (DP = 38).

5.6 Characterization of BODIPY-poly(HEMA)

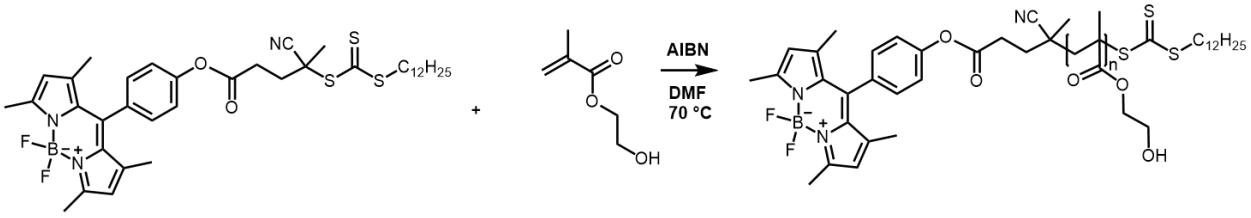

Figure S39. Synthesis of BODIPY-poly(HEMA) using BODIPY-CTA 2.

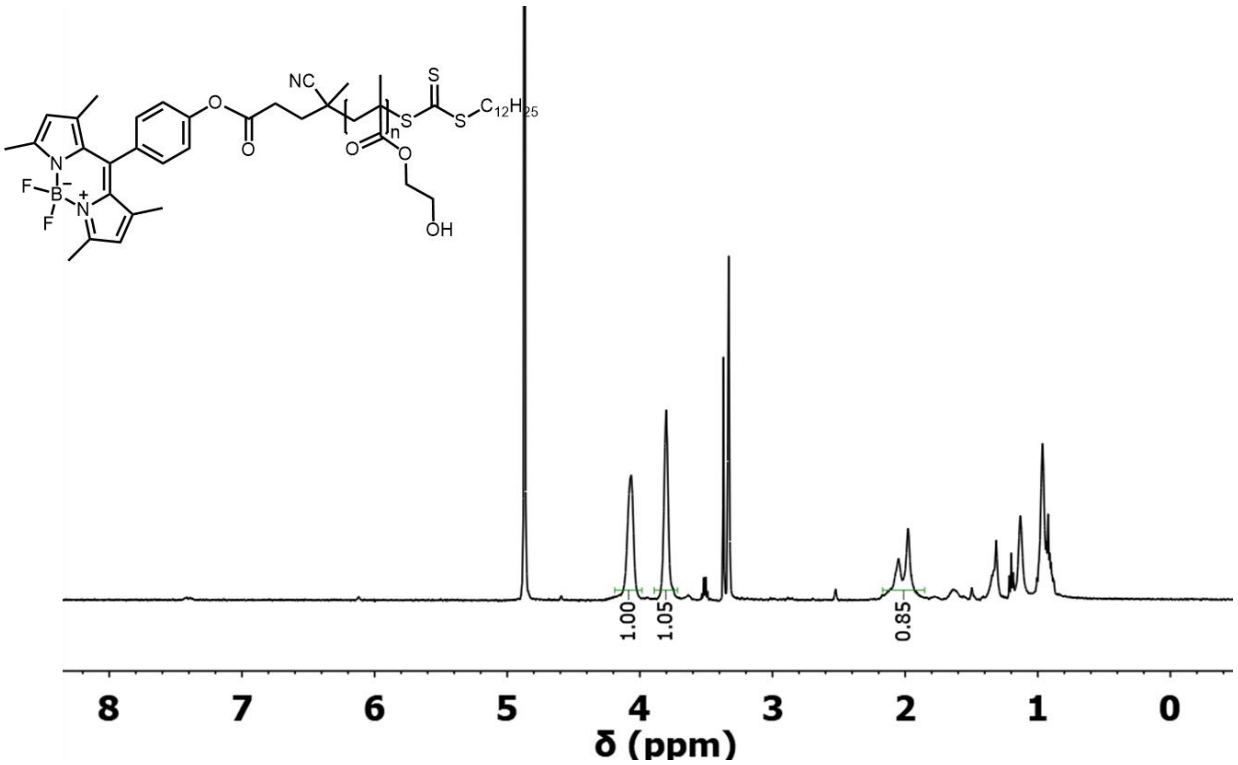

Figure S40. ^{1}H NMR of BODIPY-poly(HEMA) (DP = 50).

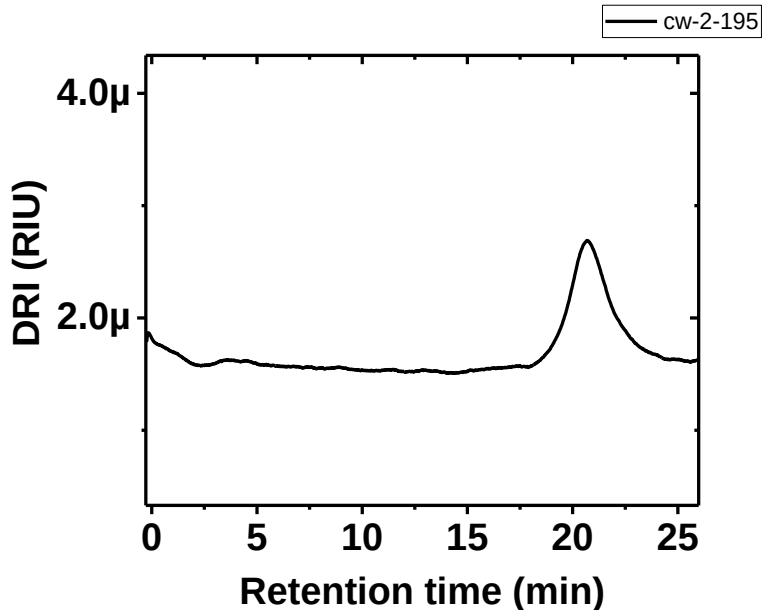

Figure S41. GPC plot of BODIPY-poly(HEMA) (DP = 50).

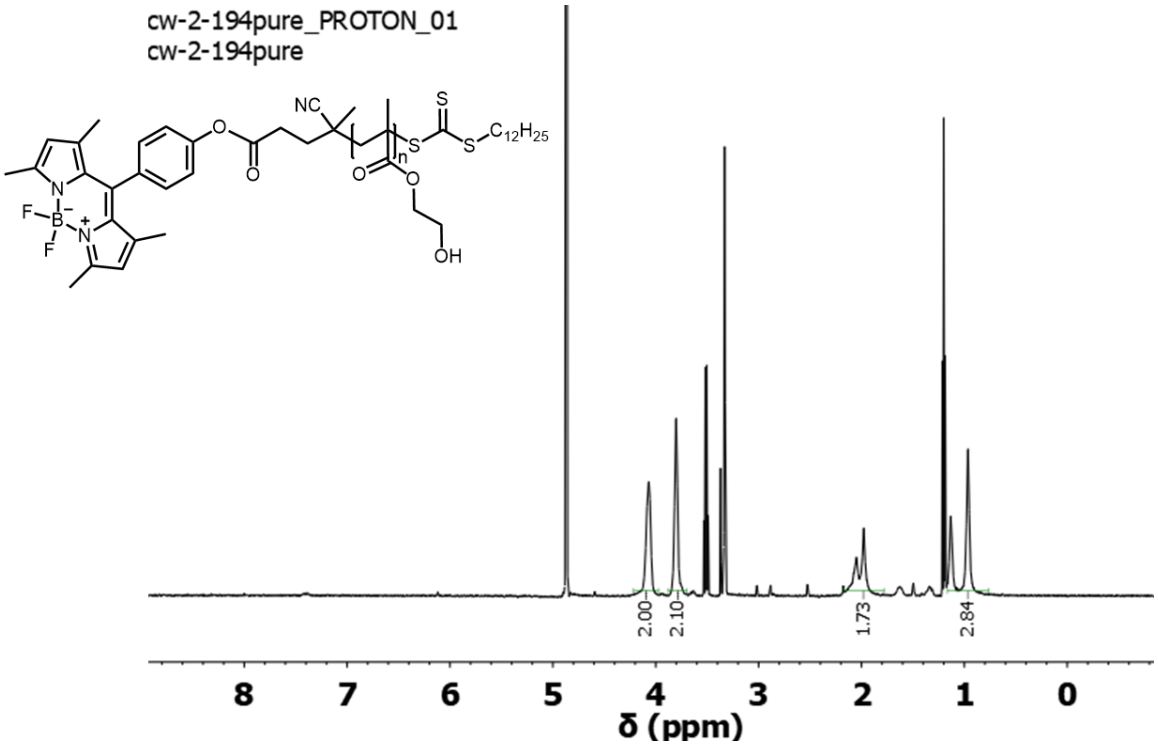

Figure S42. ^{1}H NMR of BODIPY-poly(HEMA) (DP = 90).

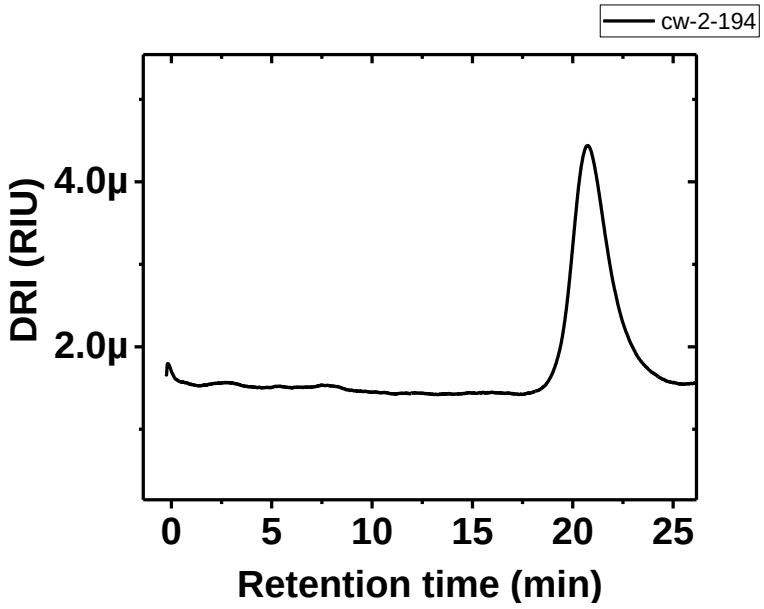

Figure S43. GPC plot of BODIPY-poly(HEMA) (DP = 90).

5.7 Characterization of BODIPY-poly(**HEMA-*r*-**AnMA)

5.7.1 BODIPY-poly(HEMA$_{46}$-*r*-AnMA$_{18}$)

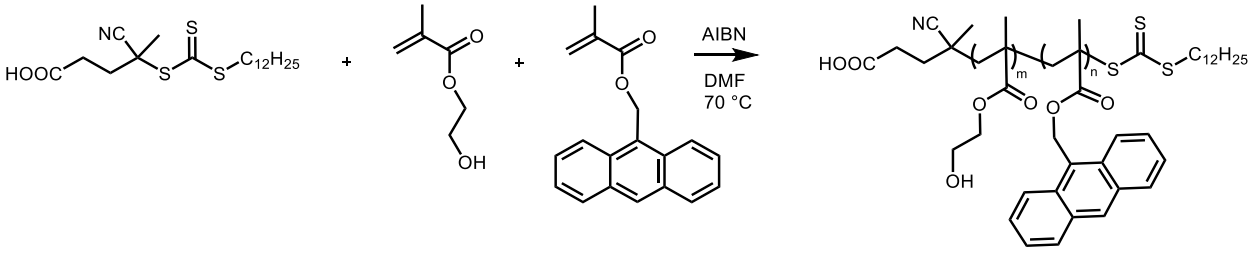

Figure S44. Synthesis of BODIPY-poly(HEMA-*r*-AnMA).

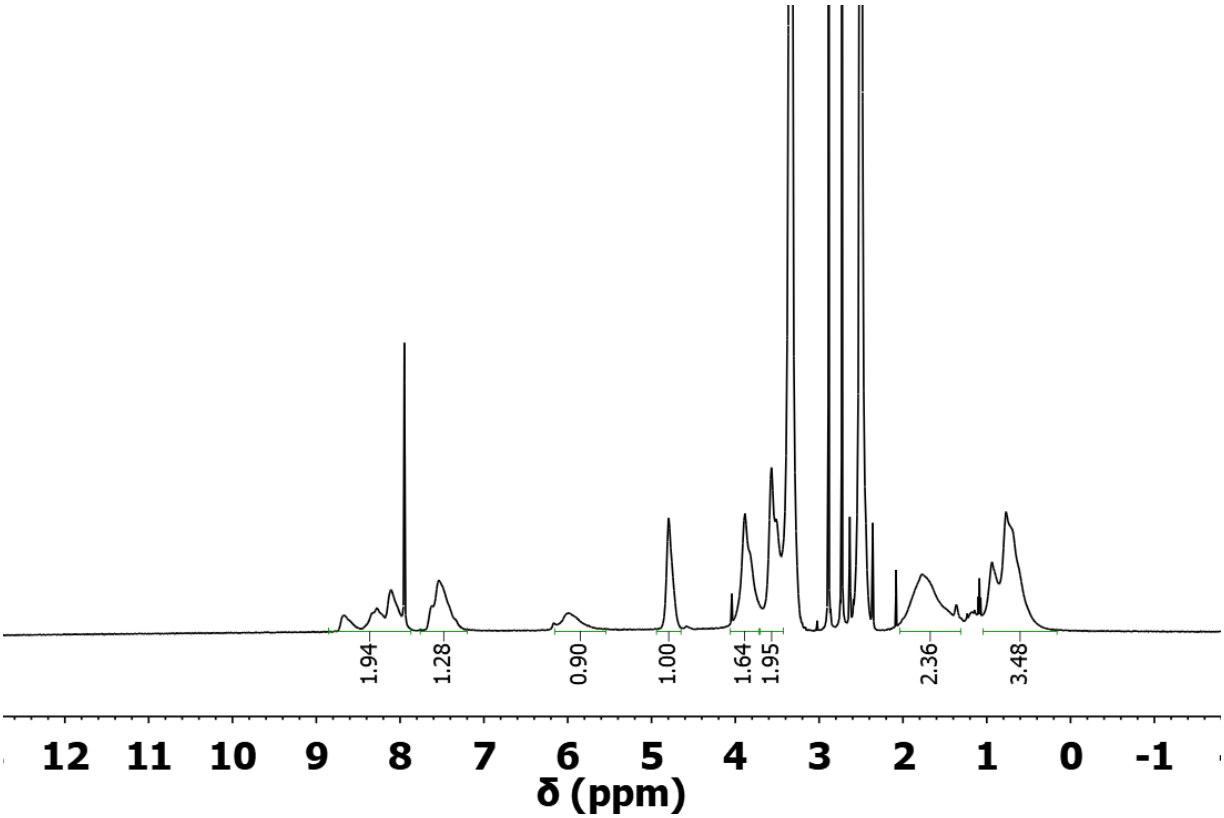

Figure S45. ^{1}H NMR spectrum of BODIPY-poly(HEMA$_{46}$-*r*-AnMA$_{18}$) in DMSO-d$_6$. This sample is hard to dissolve in methanol but soluble in acetone.

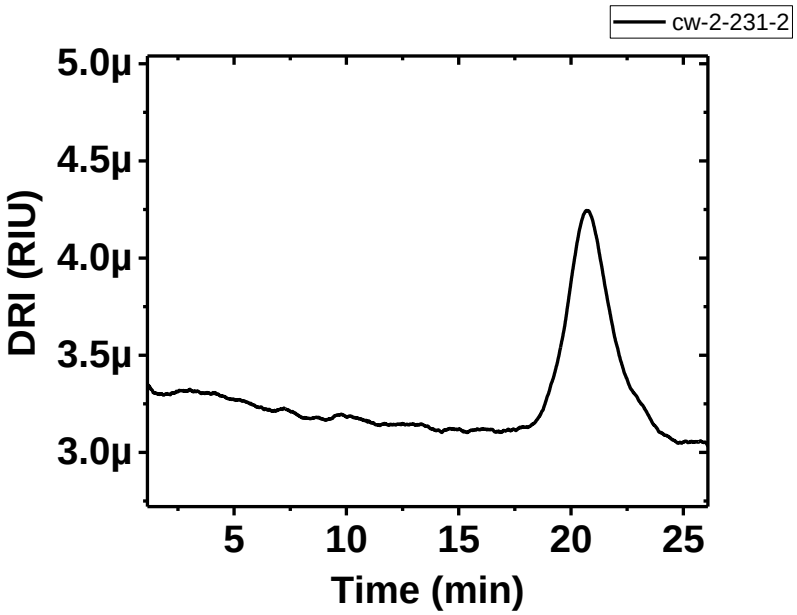

Figure S46. GPC plot of BODIPY-poly(HEMA$_{46}$-*r*-AnMA$_{18}$).

.

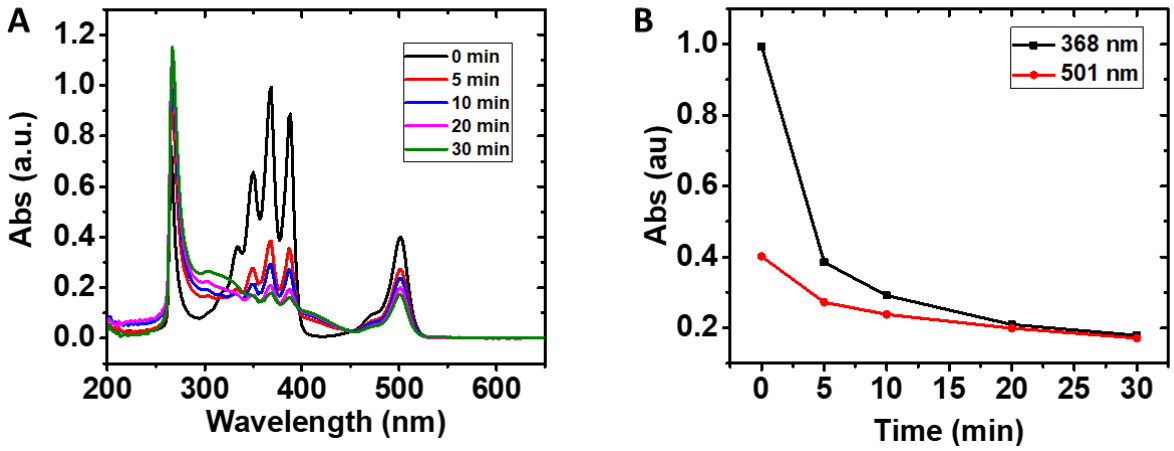

Figure S47. Photo crosslinking reaction of BODIPY-poly(HEMA$_{46}$-*r*-AnMA$_{18}$) monitored by UV-Vis spectra. 0.1 mg/mL BODIPY-poly(HEMA-*r*-AnMA) in DMF was exposed to UV (365 nm) light. UV-vis spectra were measured in DMF (0.1 mg/mL) at selected time intervals.

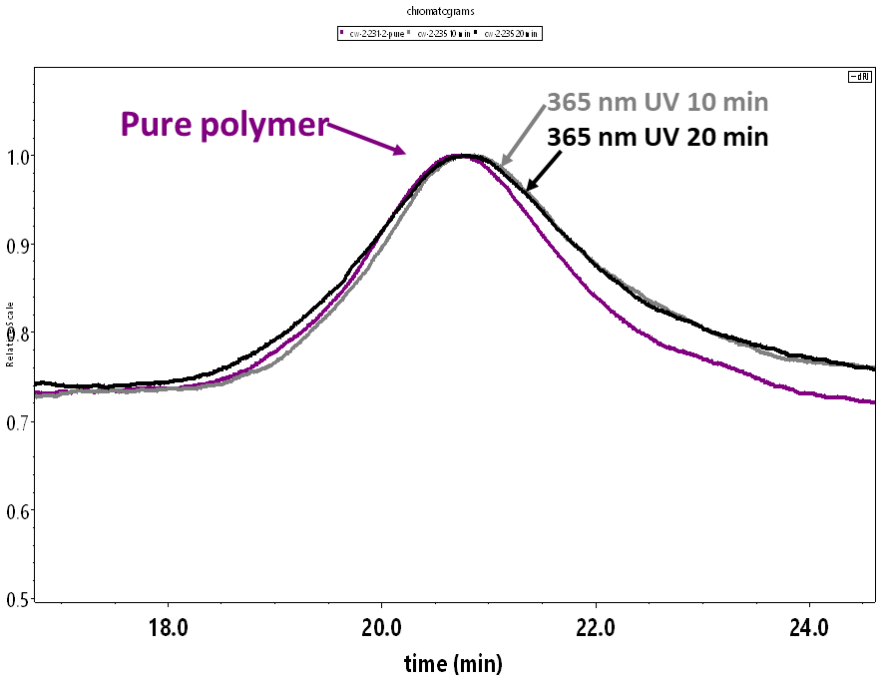

Figure S48. GPC change after 365 nm UV light radiation. 10 mg/mL solution in DMF. Retention time increased after UV radiation, suggesting that the anthracene dimerization is mostly intra chain reaction.

5.7.2 BODIPY-poly(HEMA$_{22}$-*r*-AnMA$_{23}$).

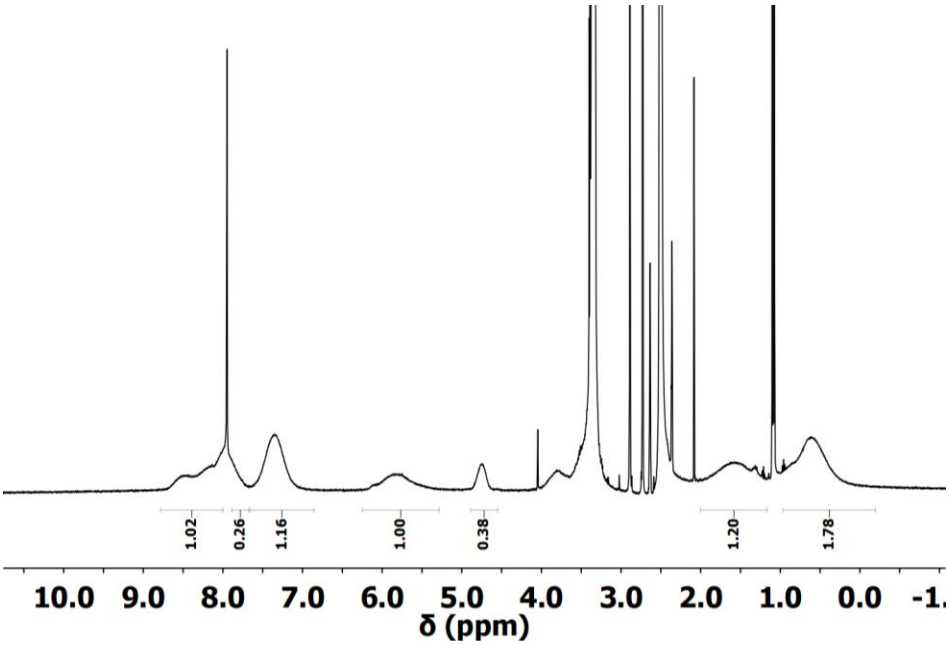

Figure S49. ^{1}H NMR spectrum of BODIPY-poly(HEMA$_{22}$-*r*-AnMA$_{23}$).

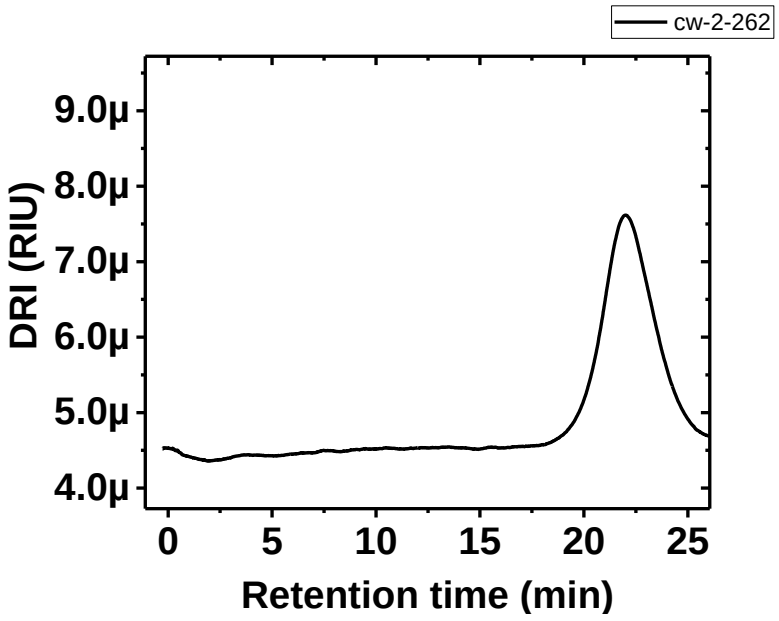

Figure S50. GPC plot of BODIPY-poly(HEMA$_{22}$-*r*-AnMA$_{23}$).

6. Glass transition temperatures of polymers used in our study.

Table S1. Glass transition temperature (T_g) of polymers of the types used in our study.[2]

Monomeric unit	T_g (°C)
butyl acrylate (C4)	-54
hexyl acrylate (C6)	-58
dodecyl acrylate (C12)	-18
2-hydroxyethyl methacrylate (HEMA)	77
2-hydroxyethyl acrylate (HEA)	-15
N, N-dimethylacrylamide (DMA)	106

The glass transition temperatures (T_g) reported in **Table S1** were measured in the absence of solvent.[2] The T_g values are expected to change substantially in nematic solvents.

7. Characterization of BODIPY-poly(alkyl acrylates) partitioned into defects

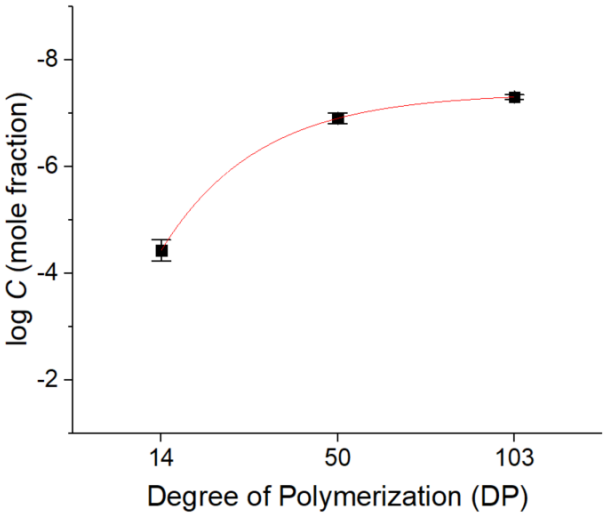

Figure S51. Threshold concentrations of BODIPY-poly(C4) at which nucleation of polymer-rich domains is observed in defects (data from Figure 3F).

The data shown in Figure S51 were fit by the equation

$$y = (-1.49) + (-2.92) * \left(1 - \exp\left(-\frac{x}{20.08}\right)\right) + (-2.92) * \left(1 - \exp\left(-\frac{x}{20.08}\right)\right) \quad \text{(S1)}$$

where x is the degree of polymerization (DP) and y is log C. When $x = 18$, we calculate

$$y = \log C = -4.95 \quad \text{(S2)}$$

which gives a predicted threshold concentration for BODIPY-poly(C4) with DP 18 of 45 μM. This threshold concentration is higher than that measured for BODIPY-poly(C6) with DP 18 (Figure 3E; 10 μM).

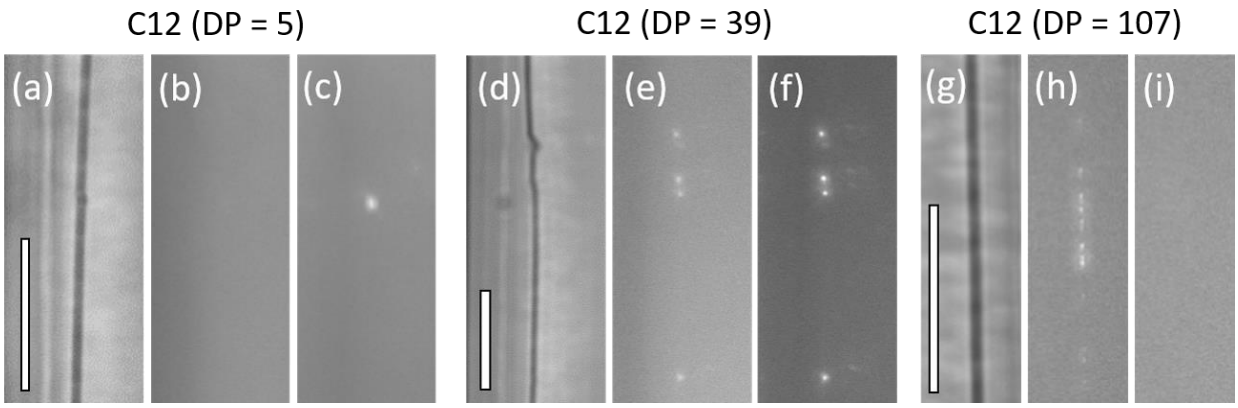

Figure S52. Fluorescence signal shifted from the dimer to monomer fluorescence with change in molecular weight of polymer (BODIPY-poly(C12)). (**a, d, g**) Bright field and fluorescence micrographs (**b, e, h**: λ_{em} 510-562 nm (monomer fluorescence); **c, f, i**: λ_{em} 606-684 nm (dimer fluorescence)) showing the distribution of BODIPY-poly(C12) in nematic 5CB.

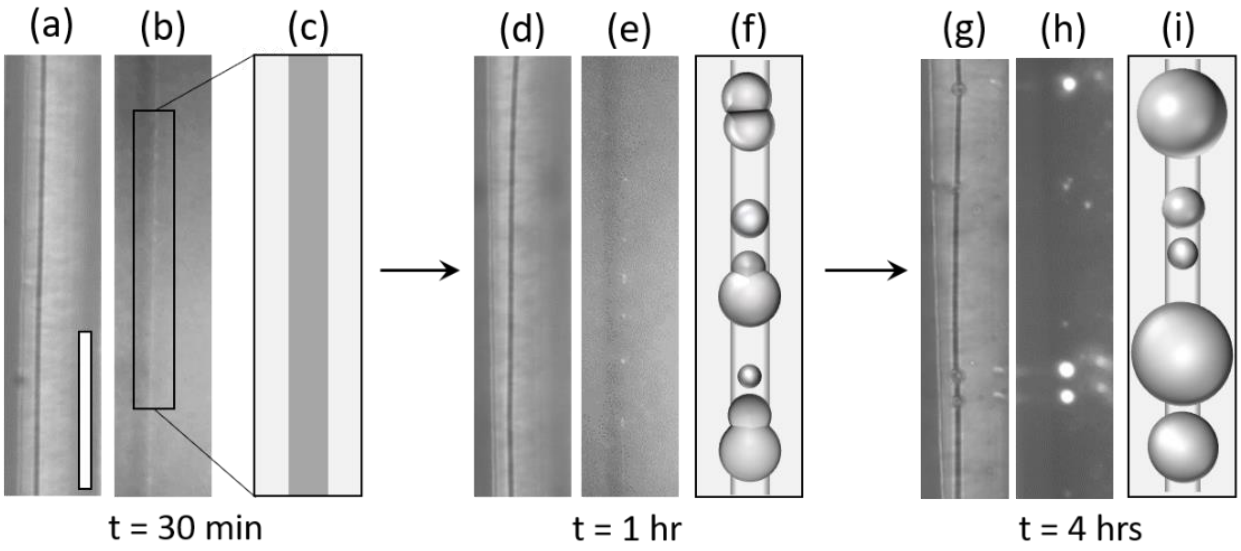

Figure S53. Nucleation and growth of polymer-rich phases templated by defects. BODIPY-poly(C6) (DP = 18) was dissolved in nematic solvent at 100 μM. **(a, d, g)** Bright-field micrographs of -1/2 disclination and **(b, e, h)** fluorescence micrographs (λ_{em}=606-684 nm; dimer signal) showing the distribution of BODIPY-poly(C6) in and around the defect. Local time-dependent phase separation within the same area of the defect were observed; **(a-c)** at t = 30 min, **(d-f)** 1 hr, and **(g-i)** 4 hrs after the nematic phase was formed. **(c, f, i)** Illustration of the initial nucleation and the growth of polymer rich phases along defects. Scale bar is 100 μm.

8. Characterization of BODIPY-poly(HEMA) partitioned into defects

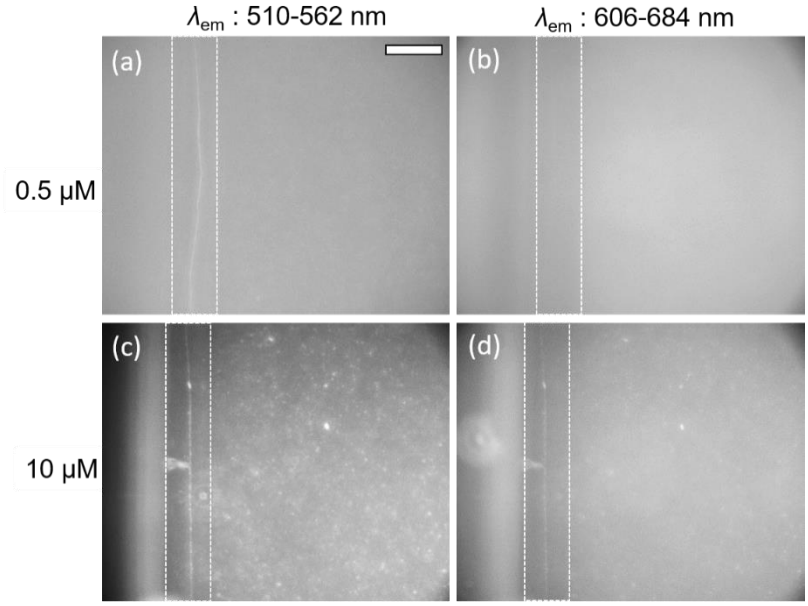

Figure S54. Difference between assemblies of BODIPY-poly(HEMA) (DP = 50) determined by fluorescence signal (**a-b**) at 0.5 μM and (**c-d**) 10 μM. (**a, c**) λ_{em} 510-562 nm (monomer fluorescence); (**b, d**) λ_{em} 606-684 nm (dimer fluorescence). The white dashed lines indicate the area where defects are located.

9. Characterization of BODIPY-poly(HEMA-*r*-AnMA) partitioned into defects

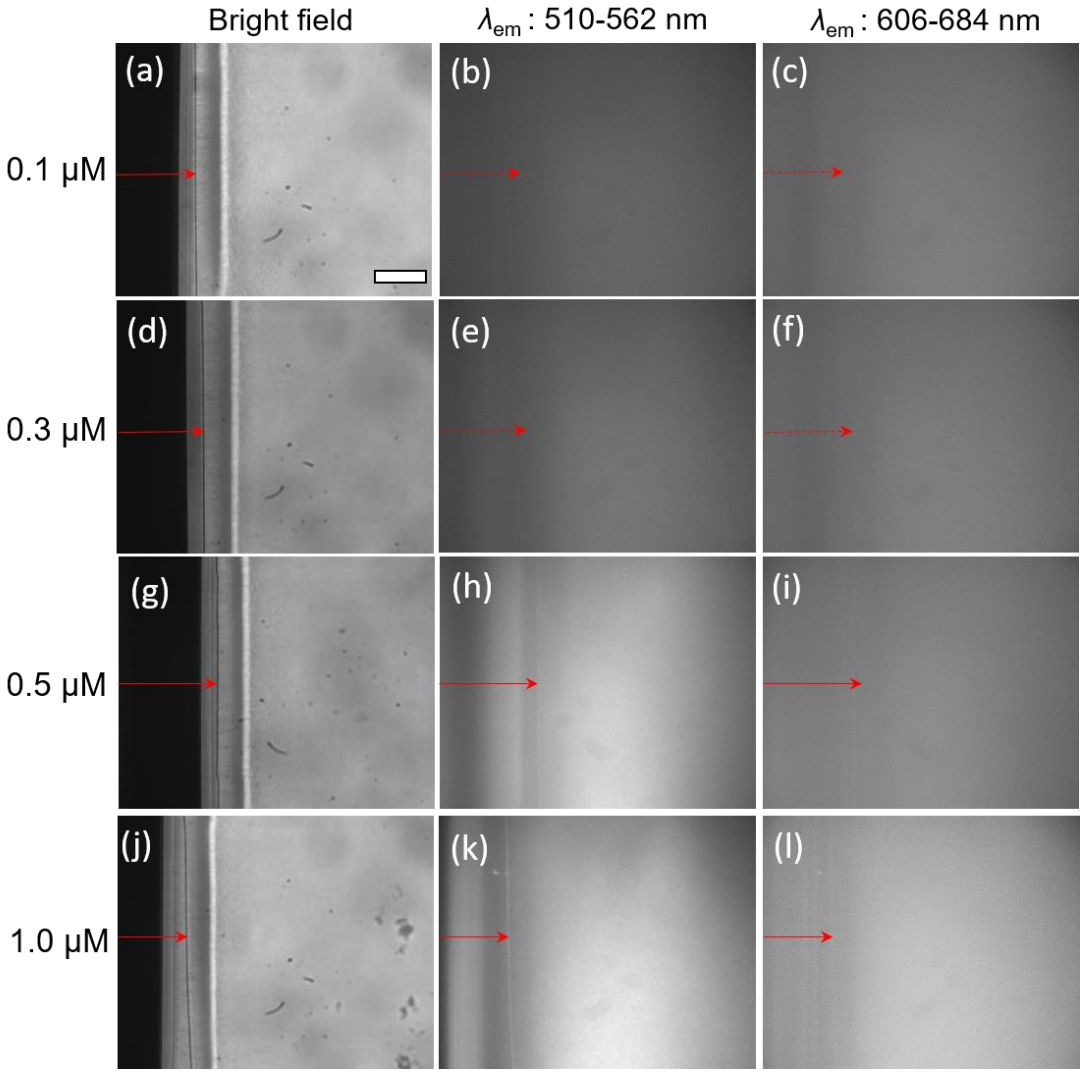

Figure S55. Determination of CAC of BODIPY-poly($HEMA_{46}$-*r*-$AnMA_{18}$) in nematic 5CB. (**a,d,g,j**) Bright field and fluorescence micrographs (**b,e,h,k**: λ_{em} 510-562 nm; **c,f,i,l**: λ_{em} 606-684 nm) showing the distribution of BODIPY-poly(HEMA-*r*-AnMA) in nematic 5CB. Red arrows indicate the locations of defects. In (**b-c**) and (**e-f**), there are no fluorescence emission in defects, but above 0.5 μM self-assembly were detected through monomer signal in (**h** and **k**). Scale bar is 100 μm.

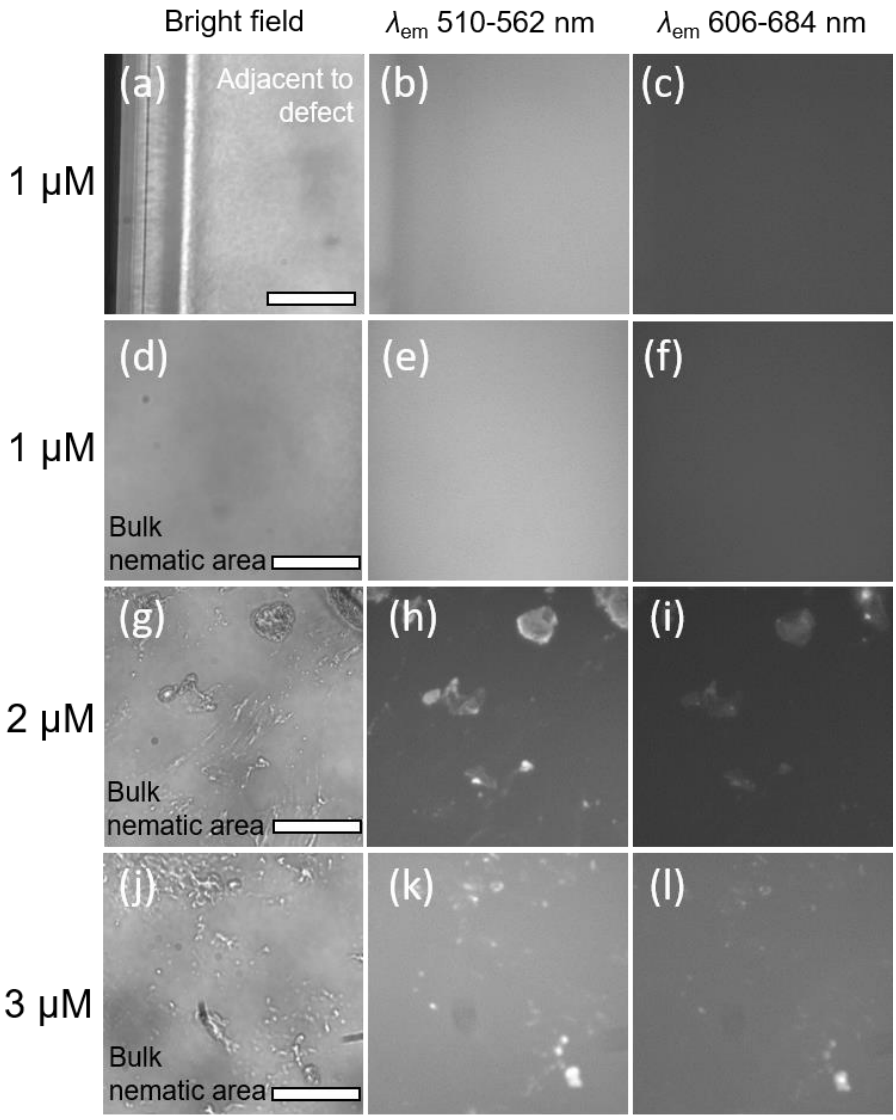

Figure S56. Bulk aggregation of BODIPY-poly(HEMA$_{22}$-*r*-AnMA$_{23}$) in nematic LCs above 2 μM. (**a,d,g,j**) Bright field and fluorescence micrographs (**b,e,h,k**: λ_{em} 510-562 nm; **c,f,i,l**: λ_{em} 606-684 nm) showing the distribution of BODIPY-poly(HEMA$_{22}$-*r*-AnMA$_{23}$) in nematic 5CB. The concentrations of BODIPY-poly(HEMA$_{22}$-*r*-AnMA$_{23}$) are indicated on the left side. (**a-c**) The region of LC with defect. (**d-l**) Bulk nematic phase, far from defect. Scale bars are 100 μm.

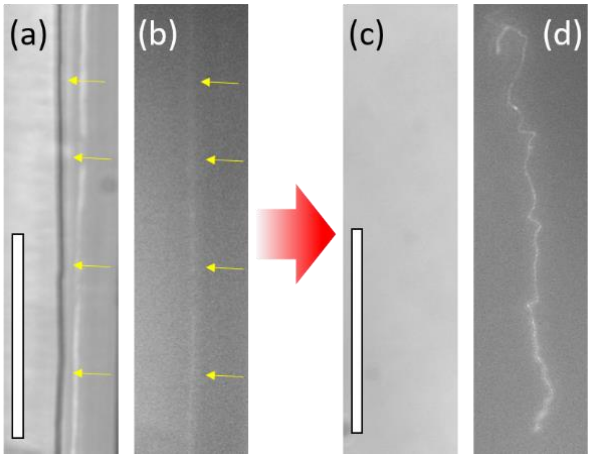

Figure S57. Cross-linking of self-assemblies of BODIPY-poly(HEMA$_{46}$-*r*-AnMA$_{18}$) templated by -1/2 defects in nematic solvents. (**a, c**) Bright field and (**b, d**) fluorescence micrographs showing the distribution of the polymer (0.7 μM in 5CB). As the nematic 5CB in (**a-b**) was heated to an isotropic state (**c-d**), the defect was removed but the cross-linked assembly was preserved and observed through monomer fluorescence signal. Scale bars are 100 μm.

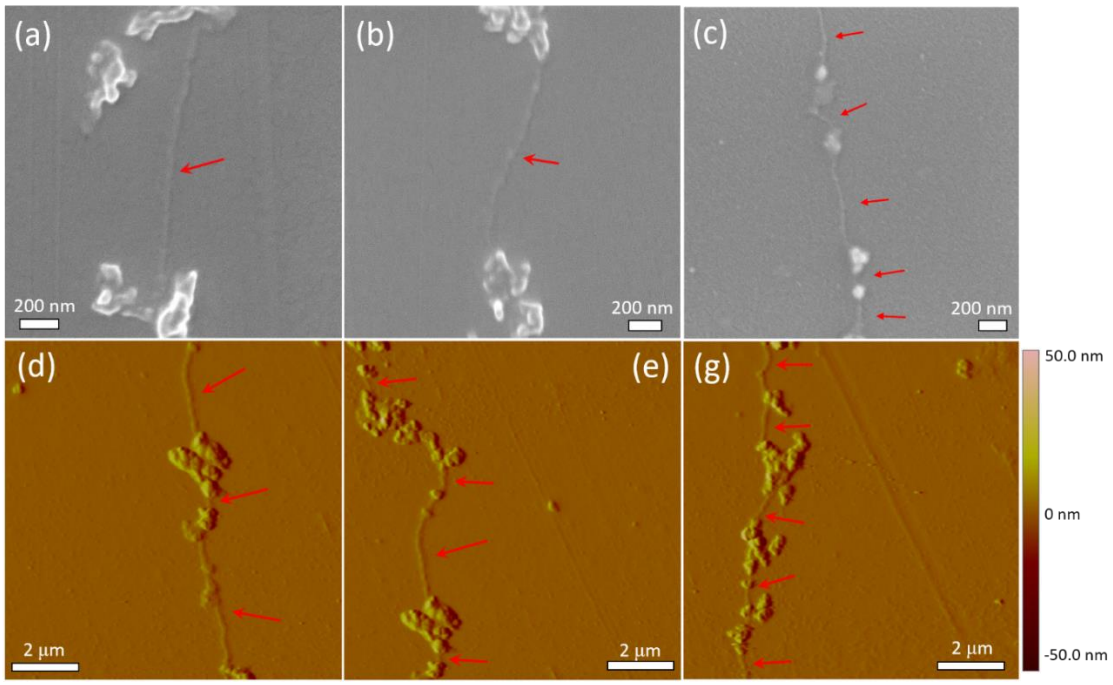

Figure S58. (**a-c**) SEM and (**d-g**) AFM characterization of cross-linked assemblies of BODIPY-poly(HEMA$_{46}$-*r*-AnMA$_{18}$) templated by -1/2 defects in nematic solvents. The initial concentration of the polymer added to nematic solvent was 0.7 μM. Red arrows indicate the formation of nanofibers, decorated by aggregates formed in bulk nematic 5CB. See main text for explanation of the rationale for deliberate introduction of bulk aggregates.

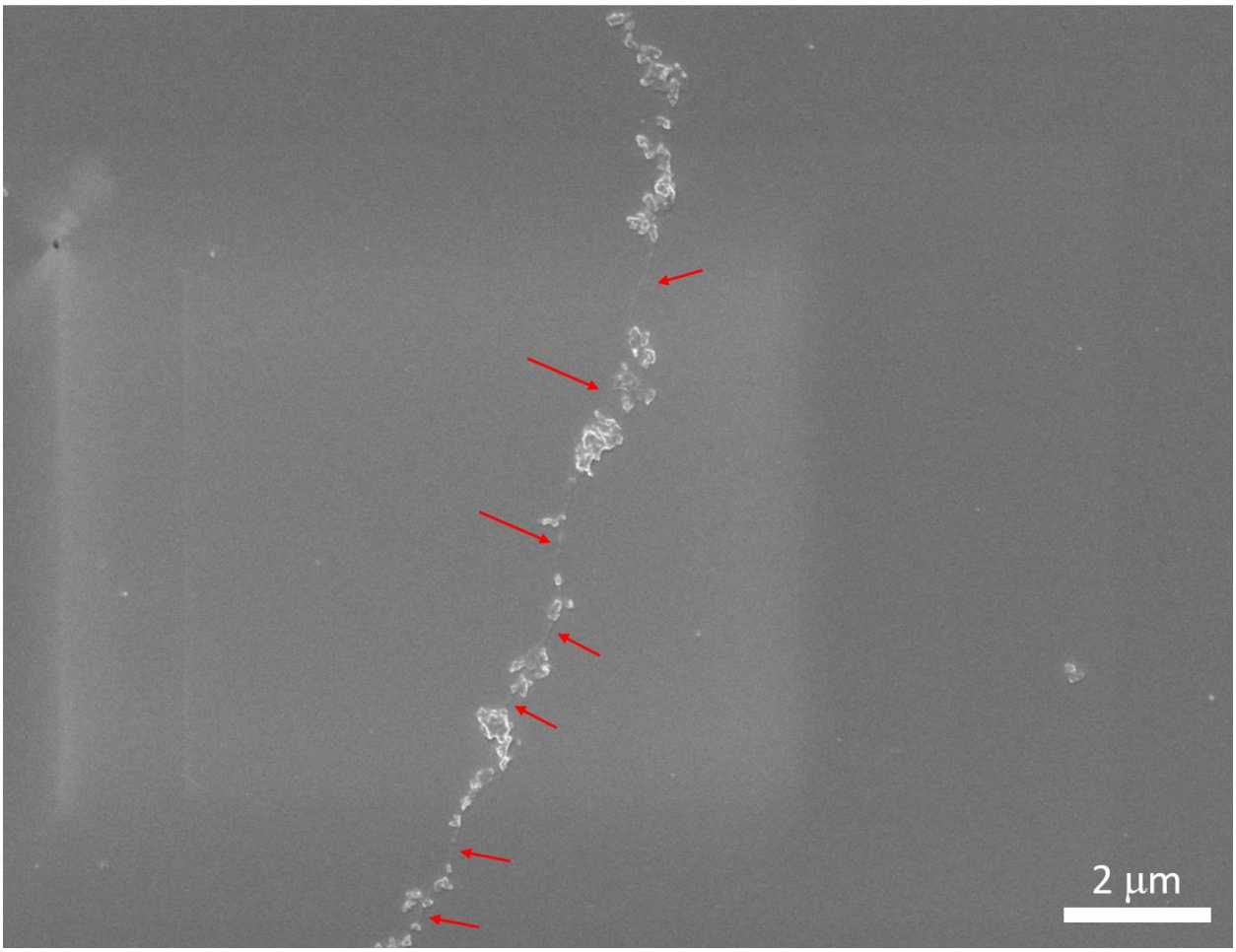

Figure S59. SEM characterization of a cross-linked assembly of BODIPY-poly(HEMA$_{46}$-*r*-AnMA$_{18}$) observed at low magnification, showing that the polymer nanofiber is longer than 20 μm in length. The initial concentration of the polymer dissolved in nematic solvents was 0.7 μM. See main text for explanation of the rationale for deliberate introduction of bulk aggregates that also decorate the defect.

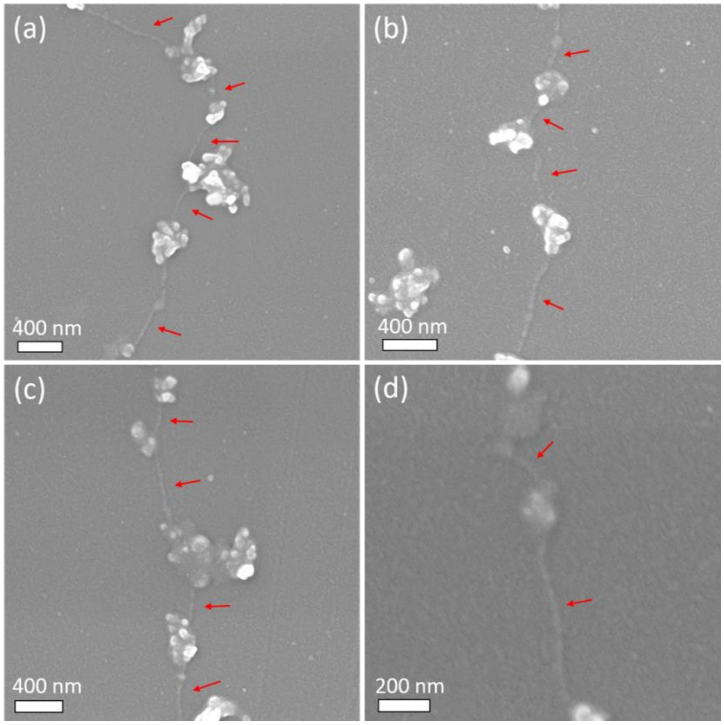

Figure S60. (**a-d**) SEM characterization of cross-linked assemblies of BODIPY-poly(HEMA$_{46}$-*r*-AnMA$_{18}$) templated by -1/2 defects in nematic solvents. The initial concentration of the polymer added to nematic solvents was 0.7 μM. See main text for explanation of the rationale for deliberate introduction of bulk aggregates, which are seen to decorate the defects in these micrographs.

10. Calculation of apparent width caused by AFM tip convolution effects

As detailed in the main text, the apparent widths of the polymer assemblies of poly(HEMA$_{46}$-r-AnMA$_{18}$) were determined to be 30 ± 5 nm and 135 ± 20 nm by SEM and AFM, respectively. We note that the larger apparent width obtained by AFM is due to convolution of the AFM tip geometry with the geometry of the polymeric assembly (**Fig. S61).** Here we calculated the apparent width caused by tip convolution as follows:

To calculate a measured width ($w_{measured}$), we can write:[3]

$$w_{measured} = 2\,(\,\Delta + r_{eff}\,) \qquad \text{(S3)}$$

where Δ represents the error due to tip convolution and r_{eff} is close to the radius of the polymer assembly (15 nm, determined by SEM), ~14 nm. To calculate the error (Δ) caused by the tip convolution, we can write:

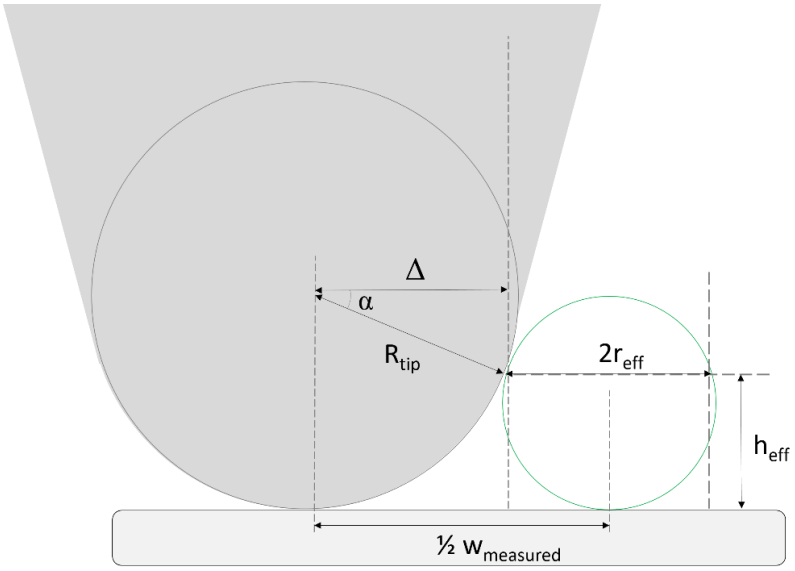

Figure S61. Schematic illustration of tip convolution effect with descriptions of a AFM tip (gray) and an object (green).

$$\Delta = R_{tip} \cos\alpha \quad \text{(S4)}$$

$$\alpha = \sin^{-1}\left[\left(R_{tip} - h_{eff}\right)/R_{tip}\right] \quad \text{(S5)}$$

where h_{eff} is effective height, defining the distance from the substrate to the contact area of the object with the tip. To calculate the effective height (h_{eff}), we can write:

$$h_{eff} = 2r_{eff} \tan 45 \sim 28 \text{ nm} \quad \text{(S6)}$$

Since the tip radius used in this study was about 30 nm, we can calculate α from equation (S5):

$$\alpha = \sin^{-1}[(30\,nm - 28\,nm)/\,30\,nm] = 3.8 \quad \text{(S7)}$$

From equation (S4), we can write:

$$\Delta = (30\,nm)\ \cos(3.8) \sim 30\,nm \quad \text{(S8)}$$

Accordingly, we obtain from equation (S3):

$$w_{measured} \approx 2\,(30\,nm + 30 \text{ nm}) = 120 \text{ nm} \quad \text{(S9)}$$

The measured width (120 nm) is in good agreement with the experimental value (135 nm ± 20 nm).

11. Characterization of BODIPY-poly(DMA) in nematic solvents

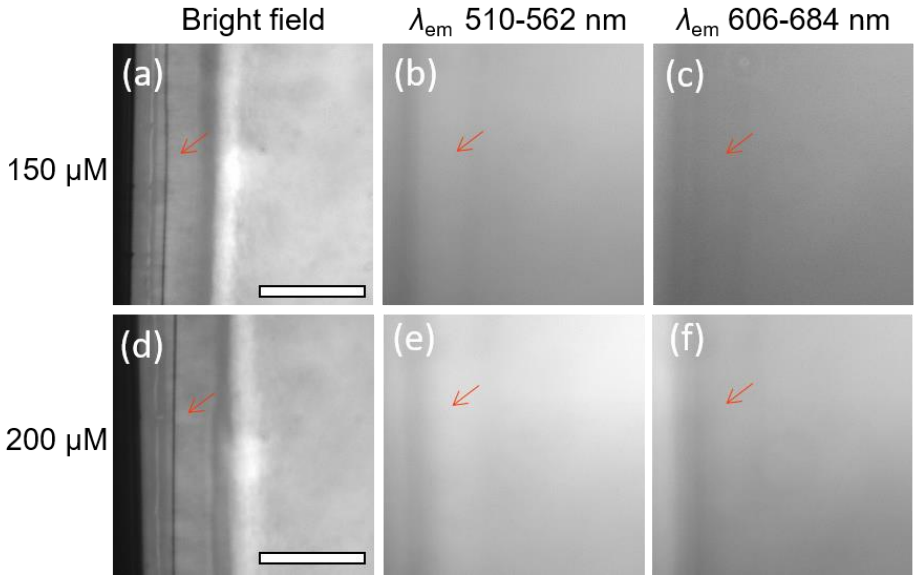

Figure S62. Dissolution of BODIPY-poly(DMA) (DP = 32) determined by fluorescence signals. (**a, d**) Bright field and fluorescence micrographs (**b, e**: λ_{em} 510-562 nm; **c, f**: λ_{em} 606-684 nm) showing the distribution of BODIPY-poly(DMA) in nematic 5CB. The concentrations of BODIPY-poly(DMA) are indicated on the left side. Scale bars are 100 μm.

References

(1) Nagai, A.; Yoshii, R.; Otsuka, T.; Kokado, K.; Chujo, Y. BODIPY-Based Chain Transfer Agent: Reversibly Thermoswitchable Luminescent Gold Nanoparticle Stabilized by BODIPY-Terminated Water-Soluble Polymer. *Langmuir* **2010,** *26* (19), 15644.

(2) Chemical Retrieval on the Web (CROW), http://www.polymerdatabase.com

(3) Canet-Ferrer, J.; Coronado, E.; Forment-Aliaga, A.; Pinilla-Cienfuegos, E. Correction of the tip convolution effects in the imaging of nanostructures studied through scanning force microscopy. *Nanotechnology* **2014,** *25* (39).